Multilayer Coatings for High-Energy Astrophysics

MIRROR SHELL 338 (Jet-X mandrel n. 8 sized - shell):

ACHIEVED TESTS AT PANTER FACILITY (MPE-Garching) AND INAF/OAB (Brera-Merate Astronomical Observatory)

INAF/OAB Internal report 02/06

Issued by *D. Spiga, D. Vernani, R. Canestrari*

Reviewed by *G. Pareschi*

PANTER measurements by *M. Freyberg, W. Burkert, G. Hartner*

Abstract

The aim of this document is the exposition of the results of full-illumination tests performed on the mirror shell 338 at PANTER X-ray facility (MPE- Garching, Germany) and results of metrological tests performed on the same shell at INAF/OAB (Merate, Italy) The mirror shell was produced (July 2005) by replication of the mandrel n.8 of the Jet-X optics mirror shell, through Au evaporation followed by Ni electroforming at Media-Lario techn. (Bosisio Parini, Italy). The resulting soft X-ray, single Au layer mirror shell was then coated with a W/Si multilayer coating at Harvard – Smithsonian Center for Astrophysics (Boston – USA) by Magnetron Sputtering, using a dedicated facility.

The multilayer coating was deposited directly on the Au coating and is structured as a double stack, constituted by two (40+7 bilayers) periodic multilayers. This simple structure – rather than the used one for astrophysical purposes, with a decreasing d-spacing through the stack – makes simpler the data interpretation.

In the following pages we will compare the mirror characteristical parameters (HEW, effective area at PANTER; figure errors, X-ray reflectivity, X-ray scattering, X-ray Diffraction, AFM/WYKO/PROMAP topography at INAF-OAB) in an overall picture and comparing to X-ray mirrors of the past. Preliminary evaluations of mirror performances for a given surface finishing level will be presented also.

Achieved tests summary

1. Mirror shell general features
2. UV optical bench (INAF-OAB) measurements – figure errors estimate
3. HEW measurements at PANTER – PSPC profiles analysis
4. Witness *XRR (X-Ray Reflectivity*) measurements at INAF/OAB –mirror shell effective area measurements at PANTER
5. *XRD (X-Ray Diffraction)* measurements at INAF/OAB
6. *AFM (Atomic Force Microscope), WYKO, XRS (X-ray Scattering)* measurements at INAF/OAB
7. HEW estimates from measured PSD (*Power Spectral Density*) from TIS *(Total Integrated Scattering*) approach
8. HEW estimates from measured PSD from convolution approach
9. Performances previsions from PSD assumptions…

1. Mirror shell general properties

mirror profile	Wolter I
average mirror diameter (parabola)	296.9 mm
average mirror diameter (hyperbola)	284.3 mm
mirror length (parabola + hyperbola)	600 mm
on-axis incidence angle	0.594°
focal length (for a source at infinity)	3.5 m
Mirror walls thickness	0.2 mm

Nominal multilayer structure (from surface toward substrate):

- **7 bilayers W/Si with constant d-spacing - period 13 nm, Γ = 0.355 (*)**
- **40 bilayers W/Si with constant d-spacing – period 3.8 nm, Γ = 0.47**
- **Au layer (200 nm)**

(*) Γ denotes the thickness ratio W/(Si+W)

From data reported above the geometrical mirror cross sections seen at PANTER can be estimated as 25.81 cm^2. This number takes into account the finite source distance. Other relevant measurement parameters have been calculated and listed hereafter.

distance source-mirror	~ 129. 5 m
beam divergence	0.065°
actual incidence angle on the parabola	0.659°
actual incidence angle on the hyperbola	0.529°
actual source image position	3.59 m
parabola lost area fraction	19.8 %
spider - vignetted area	10 -12 % (uncertain)
geometric area for single parabola reflection	6.37 cm^2
geometric area for single parabola, spider vignetted	5.6 – 5.73 cm^2
geometric area for double reflection	***25.81 cm^2***
geometric area for double reflection, spider vignetted	***22.7 - 23.2 cm^2***
radius of the parabola single-reflection corona	7 cm
radius of the hyperbola single-reflection corona	8.6 cm

2. UV optical bench measurements at INAF/OAB

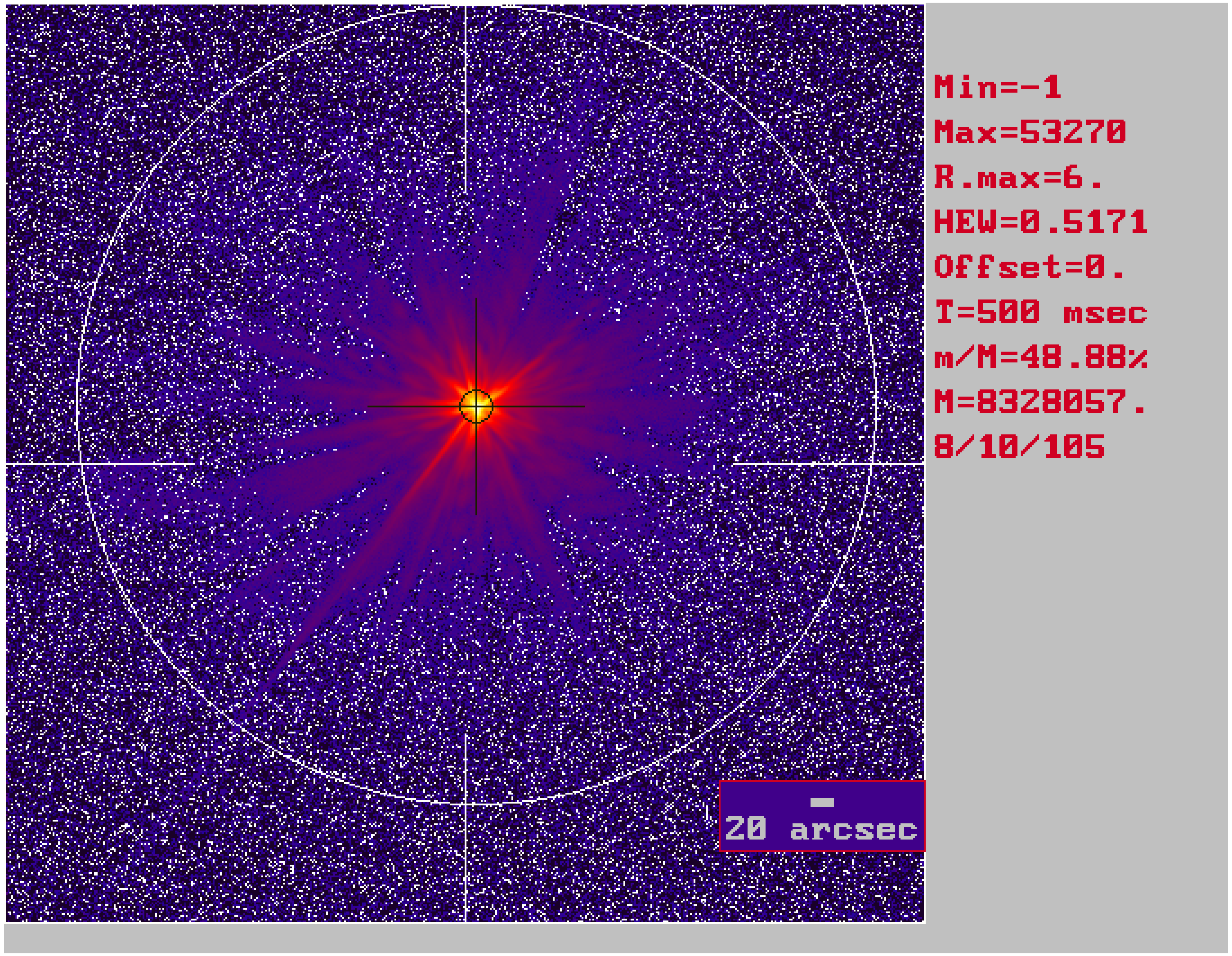

Figure errors (after 12 arms spider + case integration and UV diffract. subtract.)

HEW: 25” before measurement at PANTER

HEW: 27” after measurent at PANTER

N. B.: Rings have been left inserted in the shell (glued at three points)

For comparison : a Jet – X thin shell (130 µm thick - 24 arms spider) had HEW(1.49 keV) = 25” , while this shell has 200 µm thick walls and 12 spider arms

3. HEW measurements @ PANTER

The Half-Energy Widths of the focal spot have been measured with both PSPC and pn-CCD detectors at the following energies:

- E = 0.27 keV ➔ HEW = 45“
- E = 1.49 keV ➔ HEW = 45”
- E = 4.51 keV ➔ HEW = 55” (50 with pn-CCD)
- E = 8.05 keV ➔ HEW = 140” (72 with pn-CCD)

The discrepancy between the two instruments are caused by the small pn-CCD window that includes less scattering. The PSPC value should be considered as more significant.

In order to separate the isolate of figure errors from X-ray scattering contribution, an analysis of mirror profiles has been deal by P. Conconi (INAF/OAB): the HEW resulting contribution of figure errors are:

- HEW caused by longitudinal figure errors (measured with Long Trace Profil.): 25”
- HEW caused by azimuthal errors (measured with a roundness profilometer): 5”

Assuming a contribution of 7” caused by gravity deformations, and by summing the squared contributions OR by convolving the simulated PSF,

- total figure HEW : **27”**

We can now write that the measured PSF is the convolution of the (simulated) figure PSF with the (unknown) X-ray scattering PSF:

$$PSF_{meas} = PSF_{fig} \otimes PSF_{scatt}$$

in terms of PSF Fourier transforms,

$$\hat{F}(PSF_{meas}) = \hat{F}(PSF_{fig}) \cdot \hat{F}(PSF_{scatt})$$

By making the inverse trasform of F(PSF_{scatt}) we can recover the scattering contribution to the PSF. The resulting curves show a central core (returning a contribution of 6”, except 0.27 keV) caused by the finite PSF sampling + wings (surface X-ray scattering).

An interpretation of the HEW scattering values will be done in the last section.

PSF profile at 0.27 keV after figure errors deconvolution:

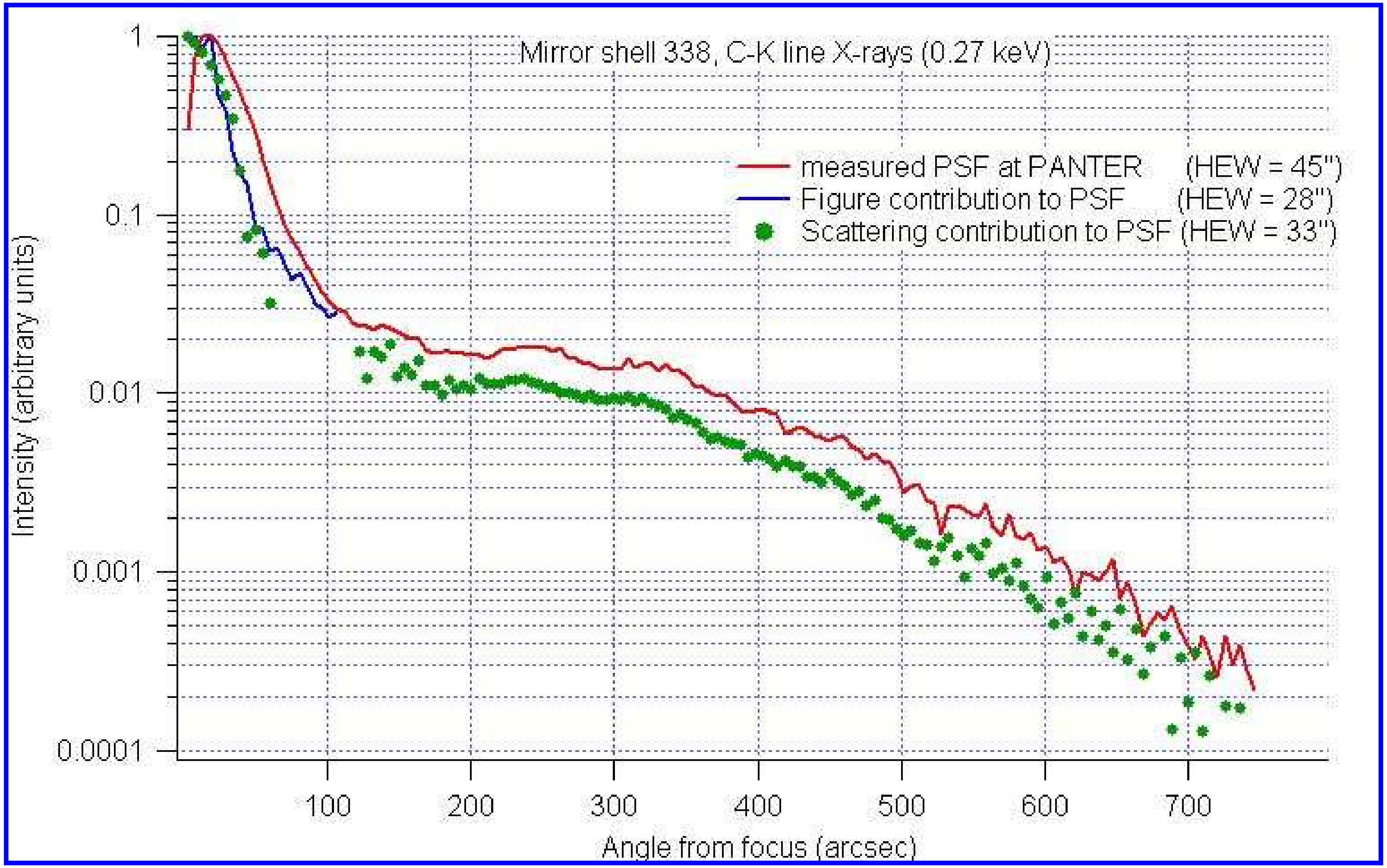

PSF profile at 1.49 keV after figure errors deconvolution:

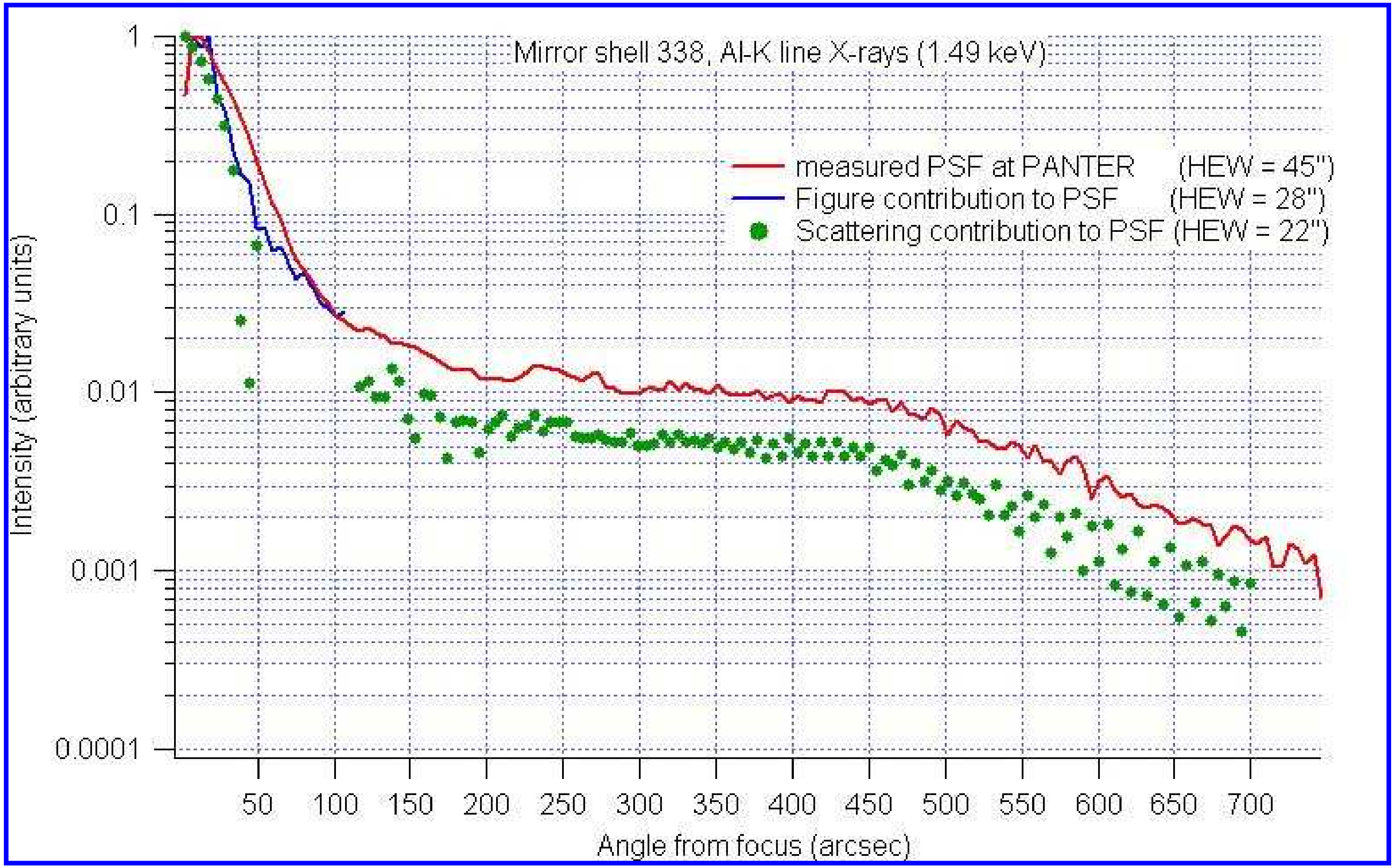

PSF profile at 4.51 keV after figure errors deconvolution:

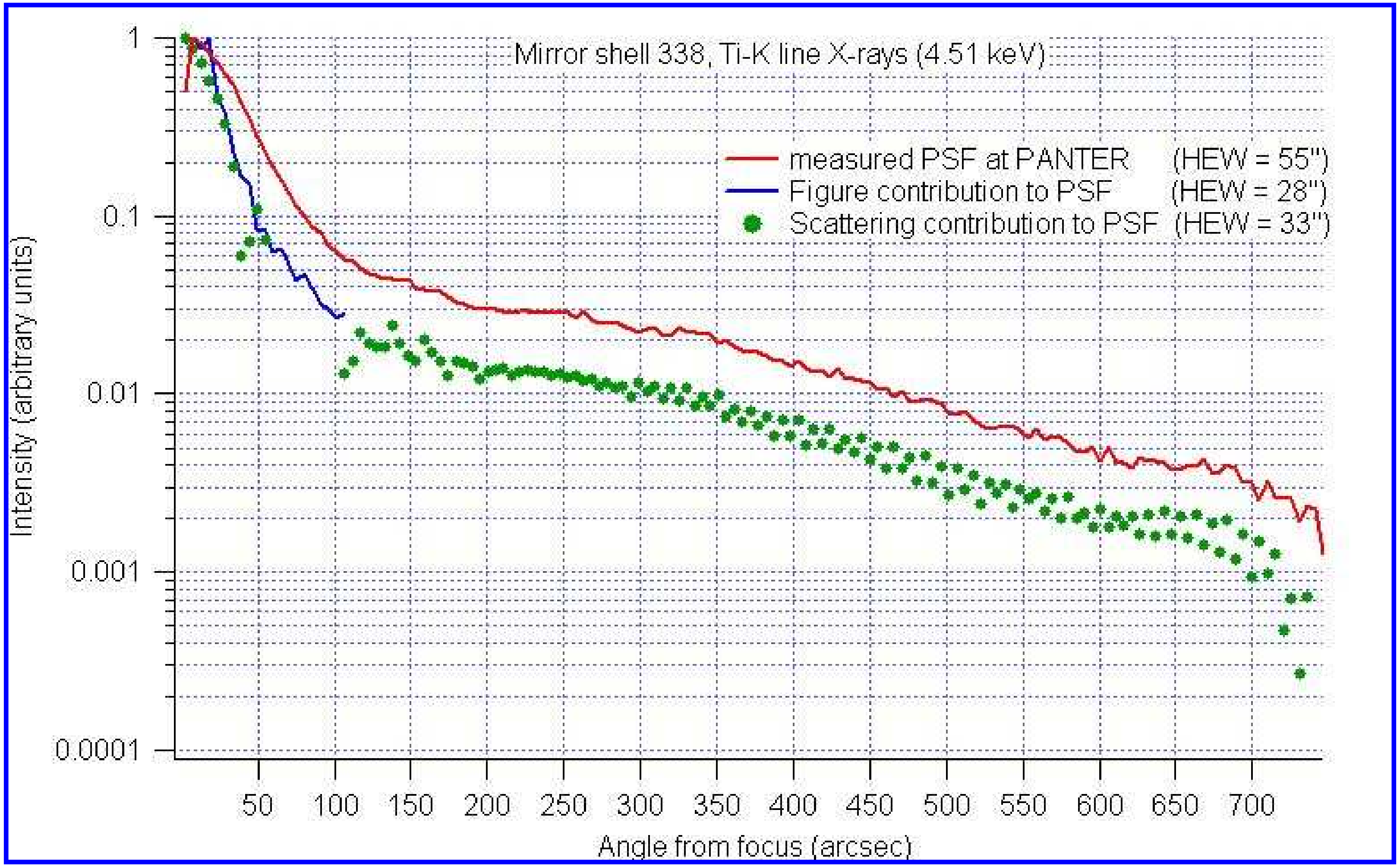

PSF profile at 8.05 keV after figure errors deconvolution:

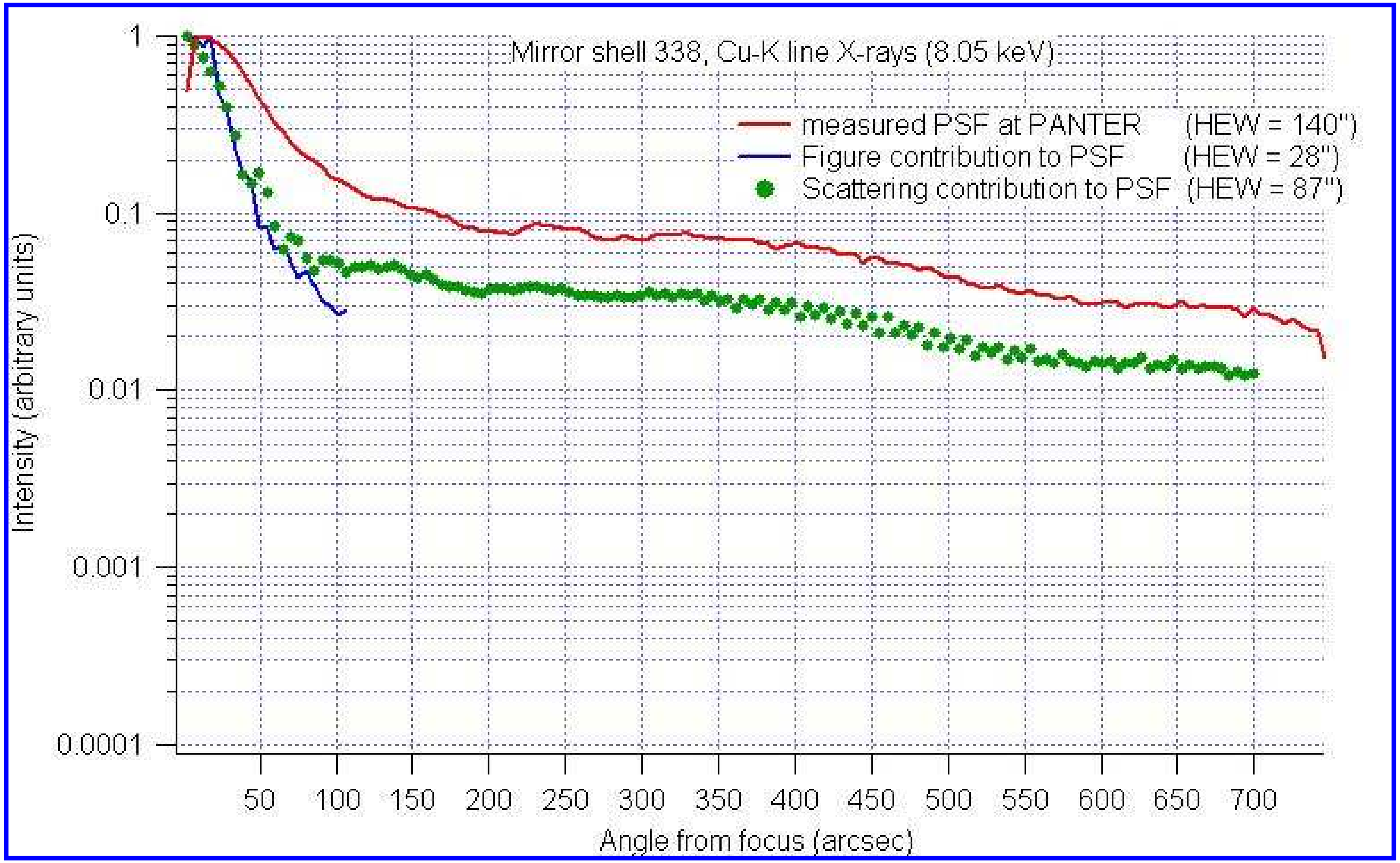

4 Effective area measurements @ PANTER

Preliminary evaluation:

- Multilayer structure has been derived from the 8.05 keV X-ray reflectivity measurement performed at OAB on the Witness mirror

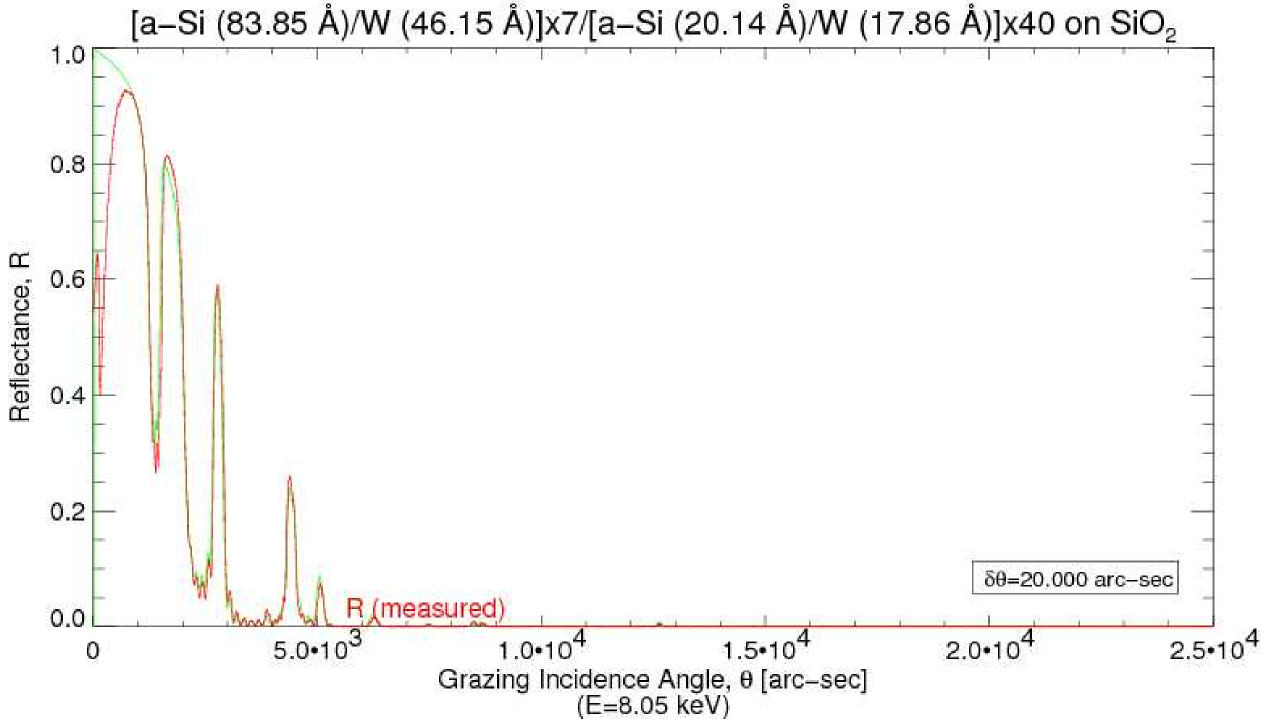

- Well-defined peaks denote a very good constance of multilayer period: the roughness rms inferred from model is 3 Å

• Two families of peaks are clearly visible in logarithmic plot: they indicate precisely the periods of two stacks (13 and 3.8 nm). Γ factors are derived from the relative heights of multilayer peaks.

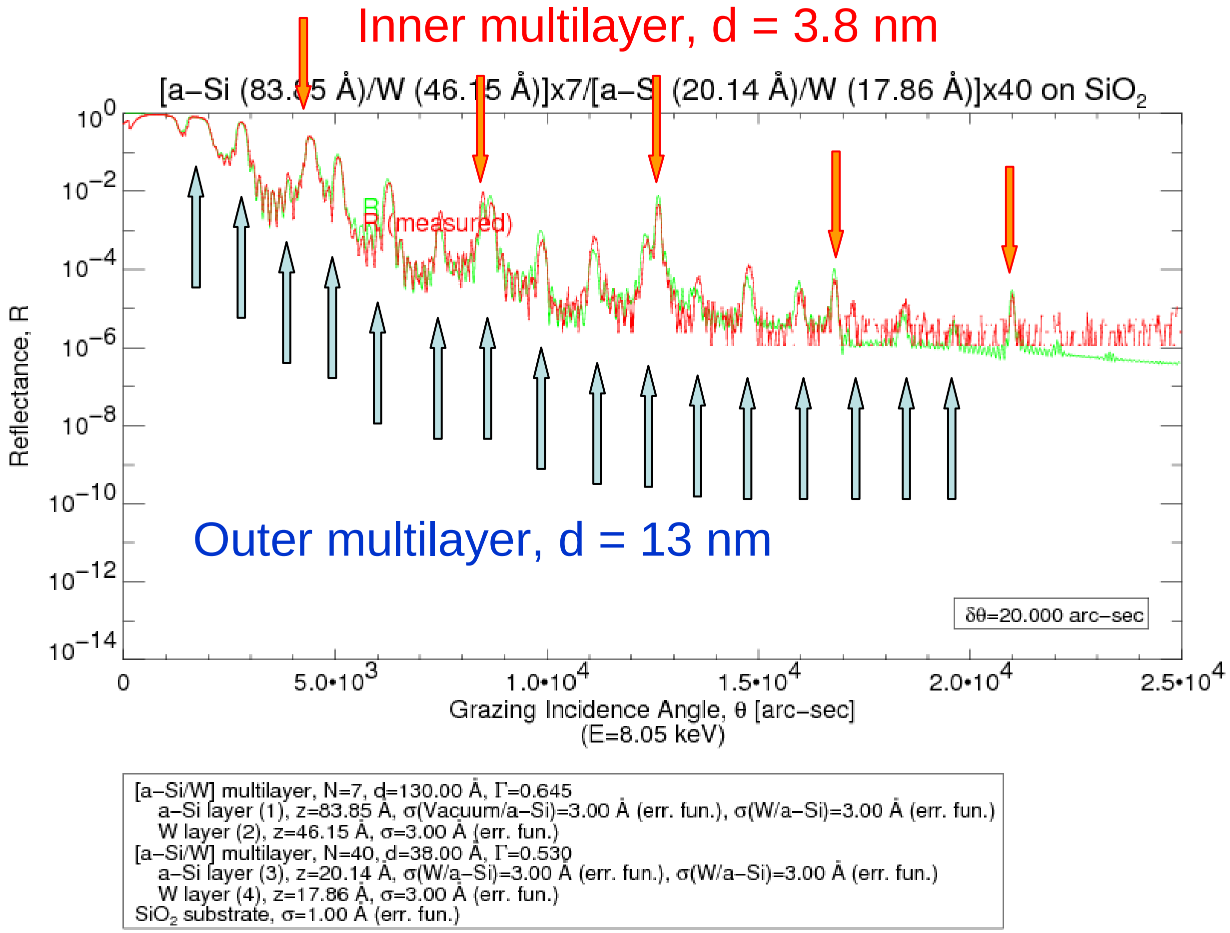

Effective area measurements have been performed at PANTER with

• PSPC (markers), in monochromatic setup

•pn-CCD camera (black line), in energy-dispersive setup, up to 12 keV

Both methods are in good agreement. The effective area has a dependence on the radius of the Region of Interest. This is caused by the large-angle scattering (out of the considered Region of Interest) from surface microroughness.

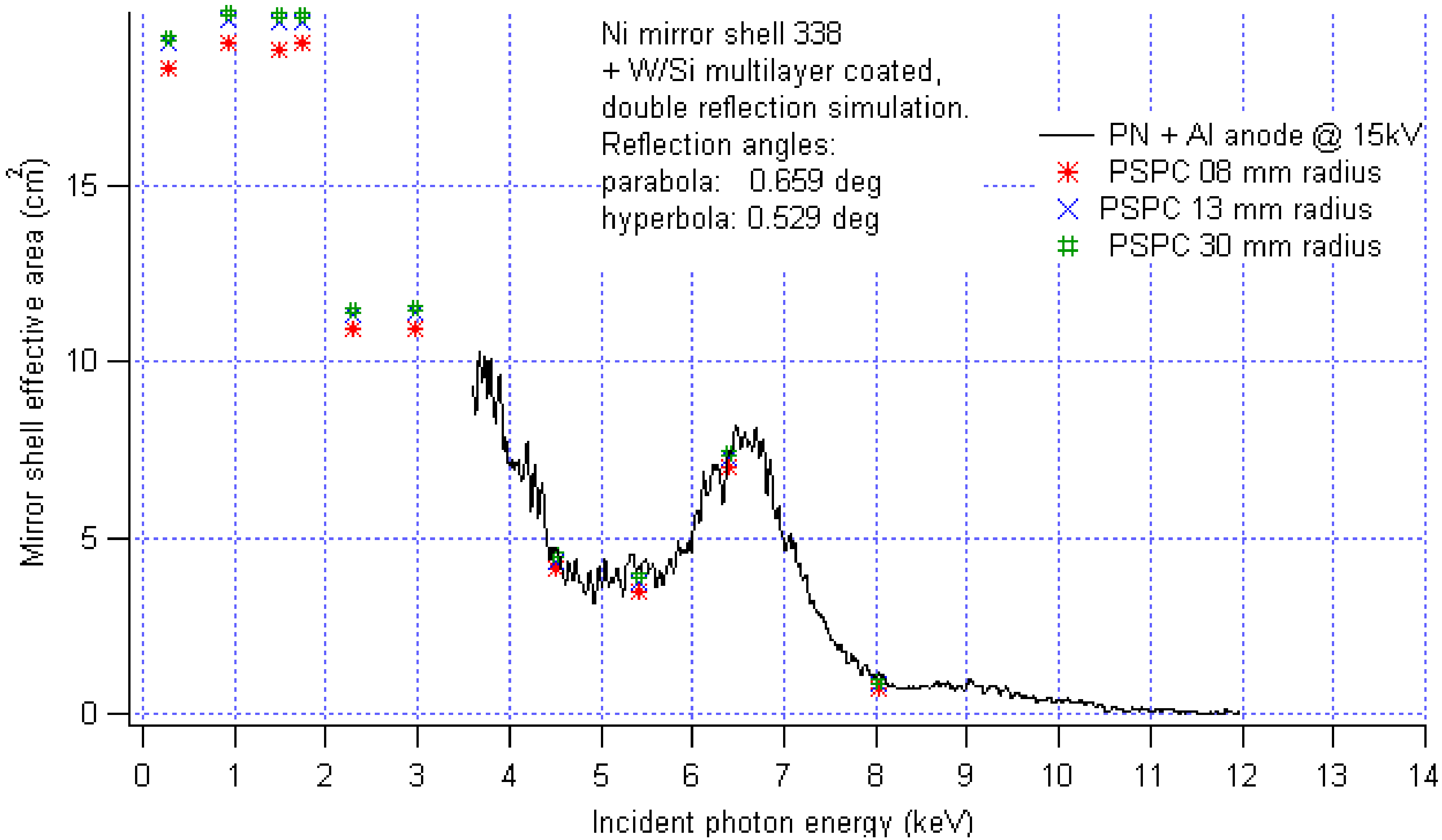

The effective area curves can be compared to the expected results from the reflectivity of multilayer as function of energy, and from the mirror geometrical cross-section for double reflection.

When dealing with this comparison, we should be aware that the incidence angles on parabola and hyperbola are different: as a consequence, Bragg peaks will be shifted and their product is very small over 12 keV.

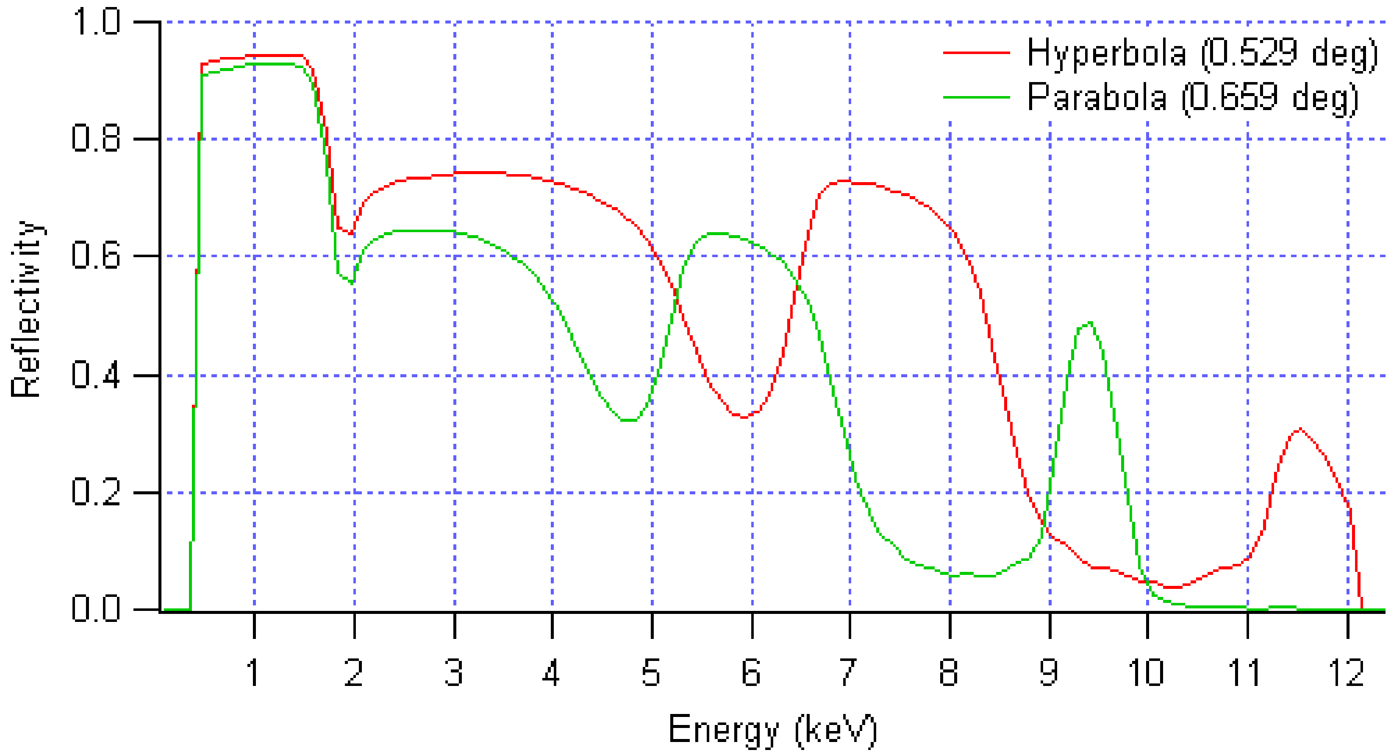

Assuming the same structure for both parabola and hyperbola multilayer (the same as witness') the effective area curves (PSPC +pn-CCD) are fitted by a model with 7 - 10 Å of roughness rms, with the exception of a maximum located at 5.5 keV, which is foreseen in model but not seen in the experiment (neither PSPC nor pn-CCD).

Note that the roughness value is strictly dependent on the measurement setup. i.e the size of the Region of Interest.

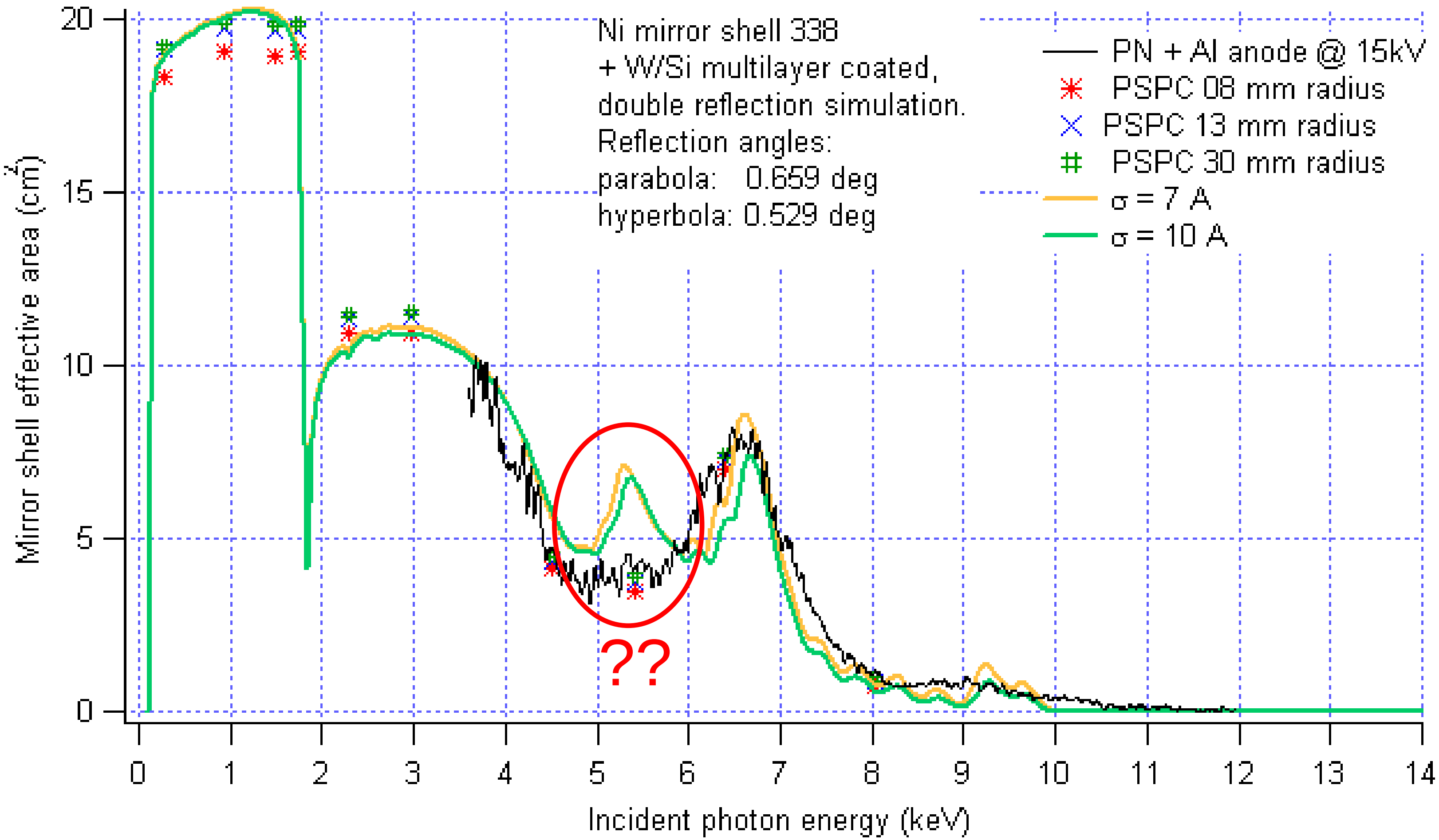

XRR measurements performed on mirror shell pieces showed that the shell multilayer has a different period from witness, and the period varies for the two reflections:

Parabola d = 11.6 nm, Hyperbola d = 14.1 nm,

This d-spacing difference allows to explain the observed discrepancy between experiment and model, because in this case the 5.5 keV peak disappears.

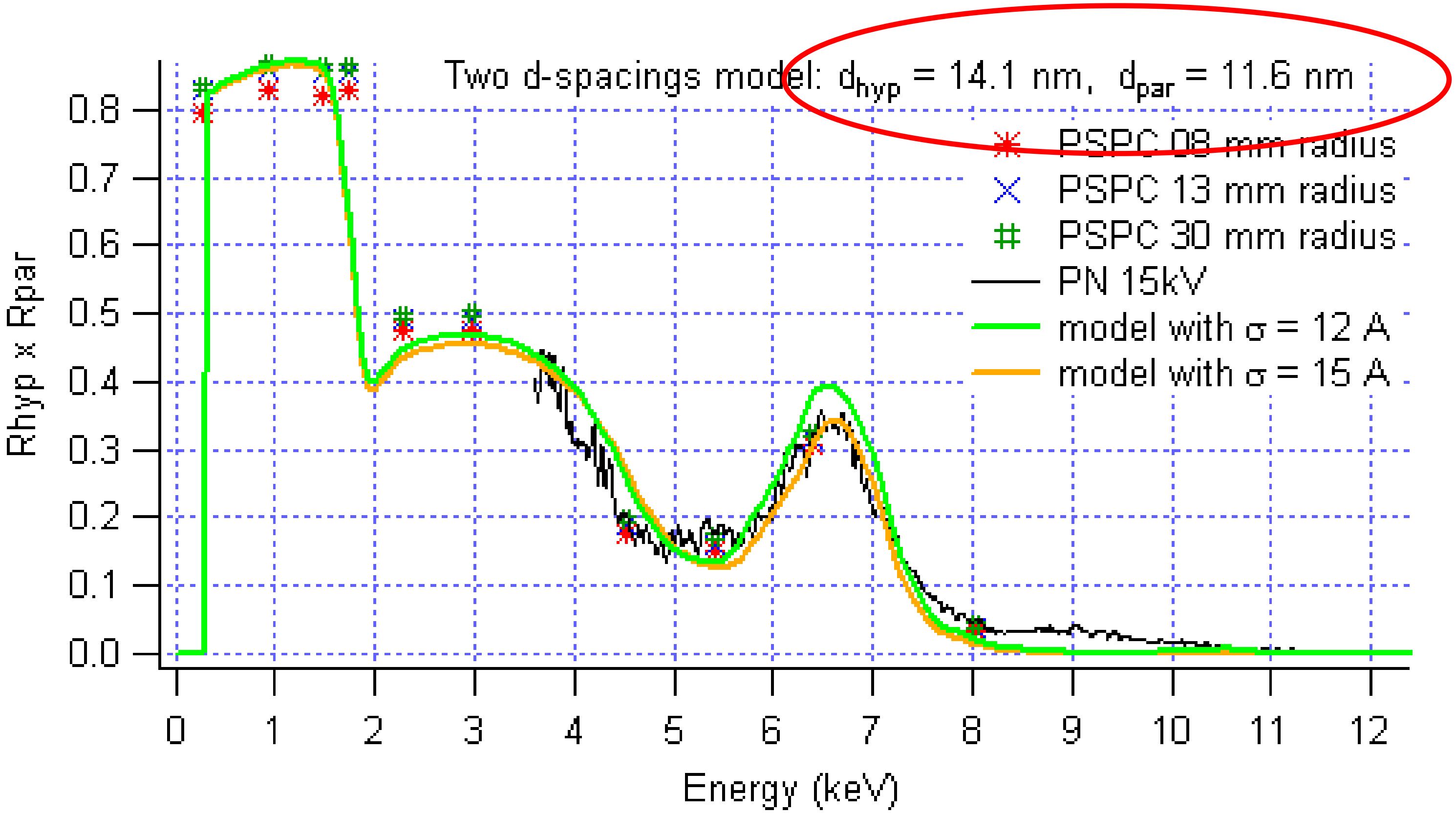

5. XRD (X-Ray Diffraction) measurements a 8.05 keV

In order to explore the presence of microcrystal in multilayer structure, we searched for diffraction peaks in a reflectivity scan at large angles. Peaks on the XRD scan were observed at 19° and 22.2°, and they are interpreted as diffraction peaks from Au and Ni crystals (analysis by D. Vernani).

d_{111}(Au) --> $\theta \sim 19°$ d_{200}(Au)--> $\theta \sim 22.2°$ d_{111}(Ni) --> $\theta \sim 22.2°$

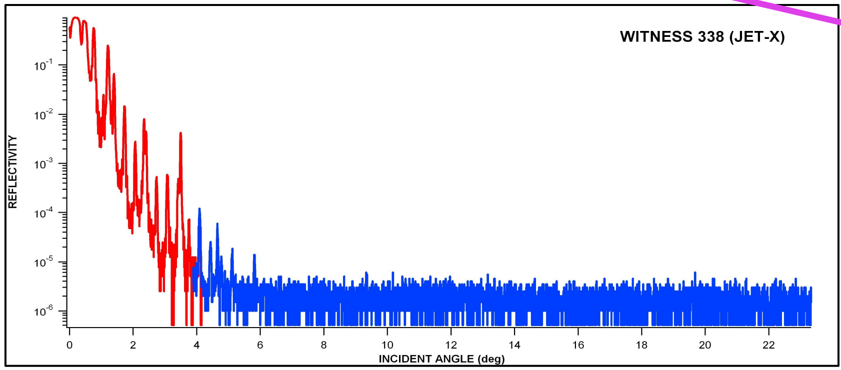

Witness (multilayer + glass)

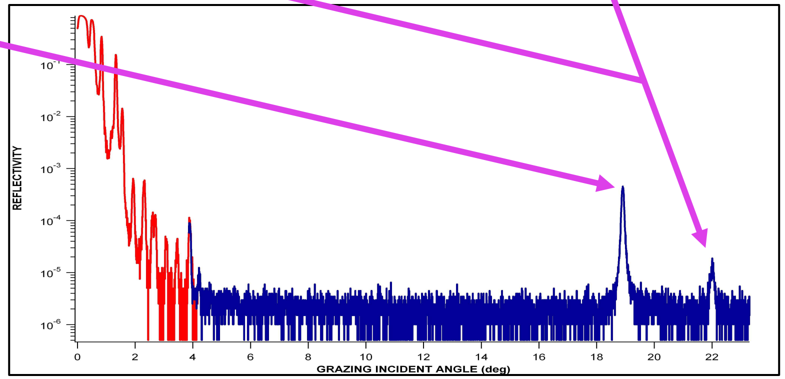

Shell (multilayer + Au + Ni)

No XRD peak was observed for eventual crystals of:

- W, at 24.9° <111>, and 29.1° <200>
- WSi_2, at 13.85° <100>, 15° <101>, 19.8° <110>, e 21° <111>

that would indicate a multilayer amorphous microstructure.

6. Topographical and XRS measurements of witness mirror and mirror shell samples

WITNESS 338

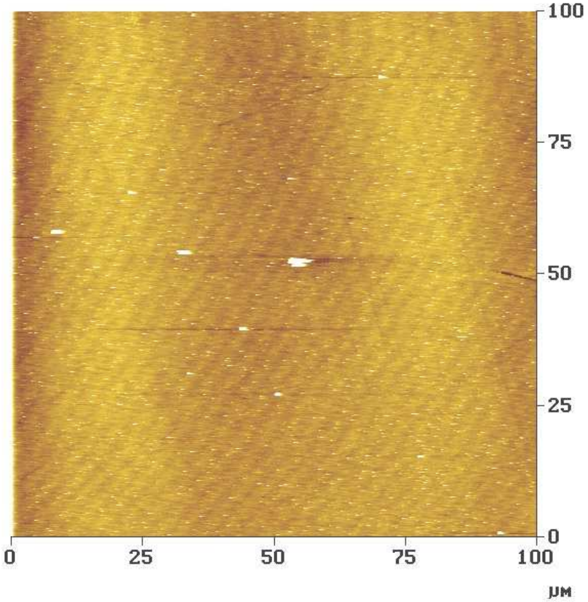

100 μm

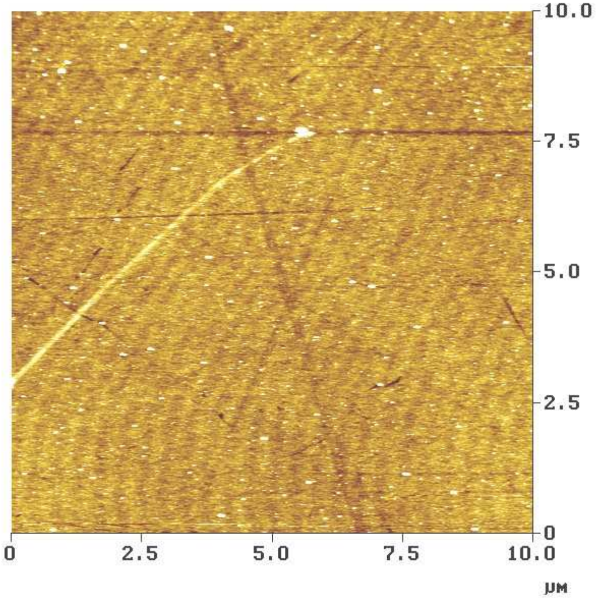

10 μm

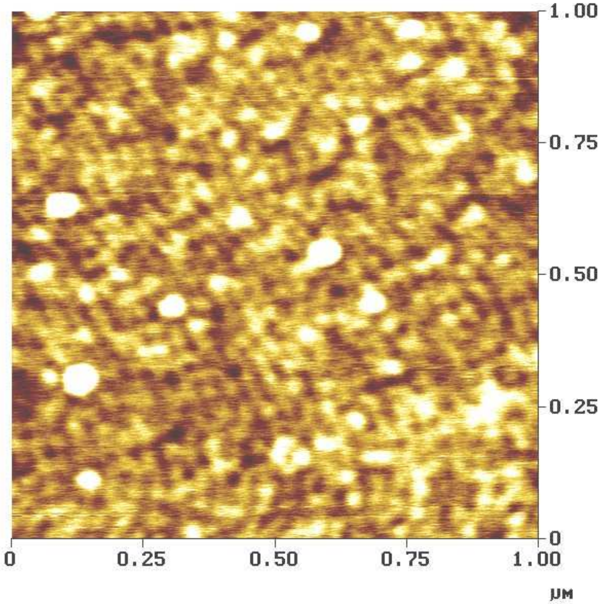

1 μm

Measured roughness**:**

σ_{100} **= 2.8 Å** σ_{10} **= 2.9 Å** σ_1 **= 2.0** Å

σ_{total} = 3.19 Å

MIRROR SHELL 338 – Au substrate

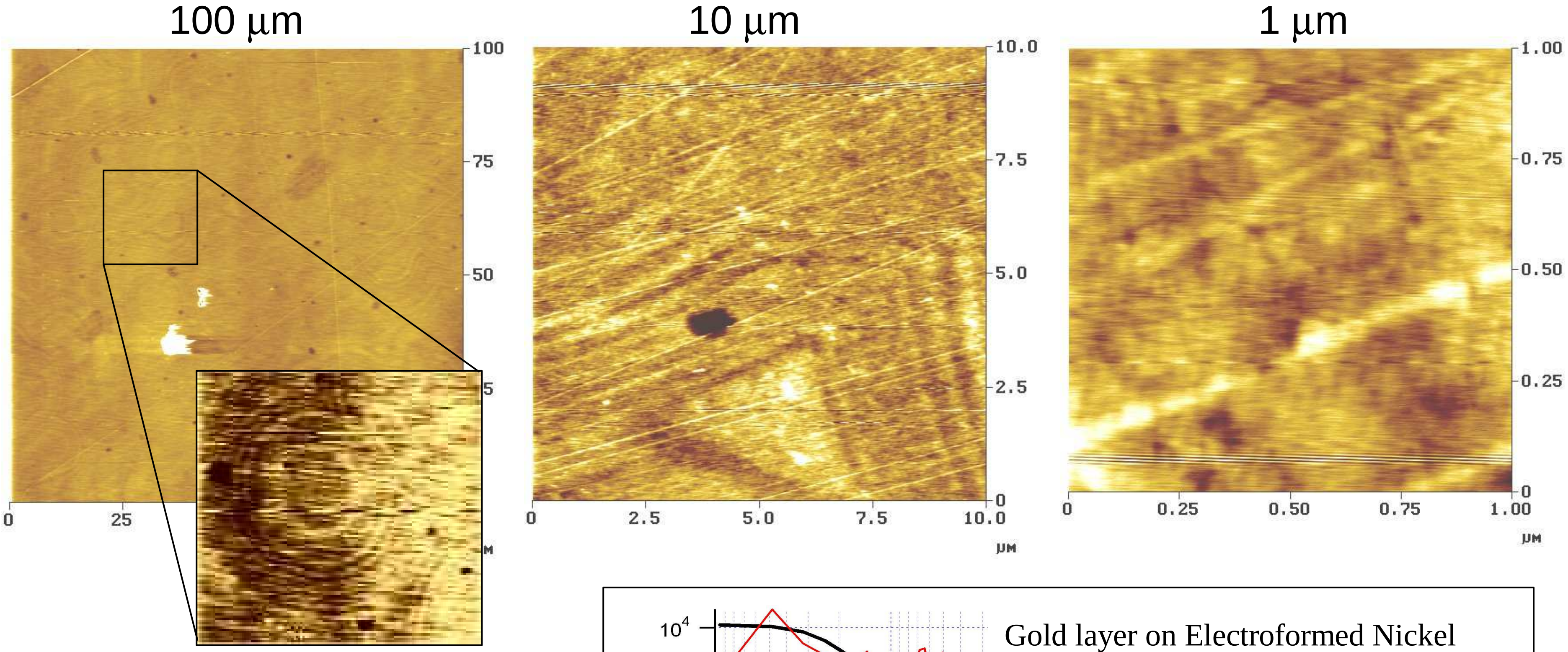

Circular structures of some 10 mm diameter appear on the Au surface. The corresponding surface rms are listed aside. The surface PSD is also shown.

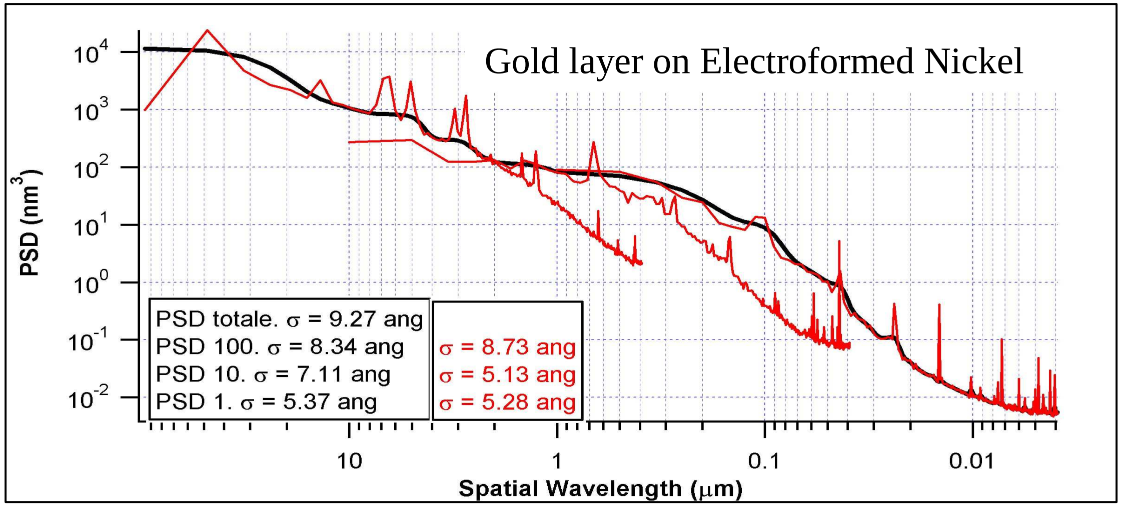

MIRROR SHELL 338 – multilayer surface

100 μm

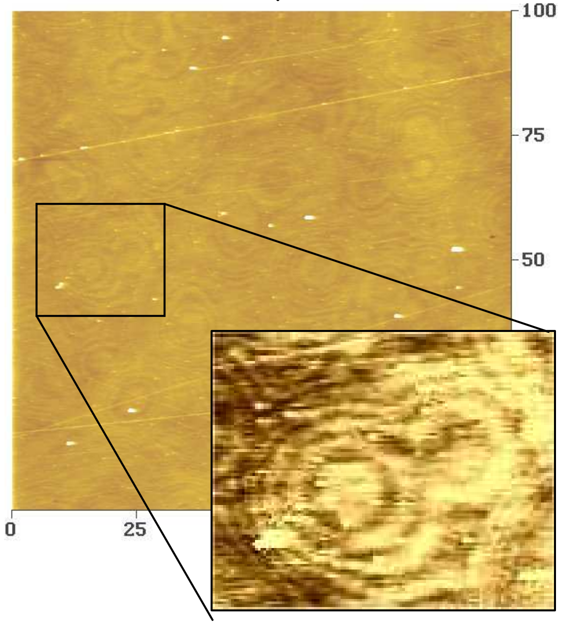

10 μm

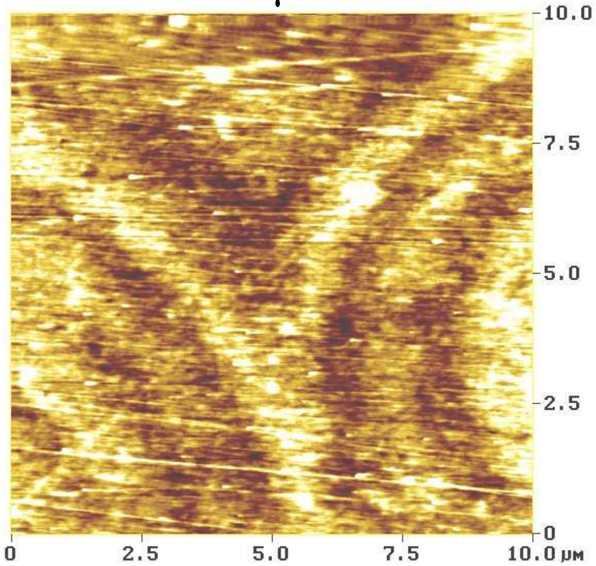

1 μm

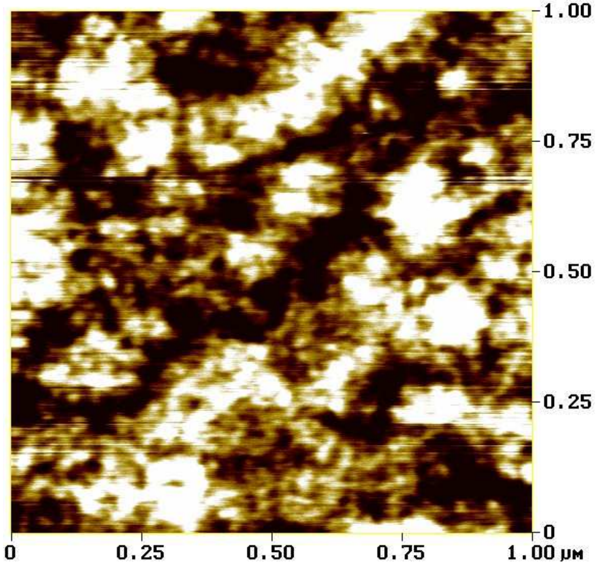

The same circular structures are printed through the multilayer coating. The surface roughness (see aside) is almost the same as the Au substrate.

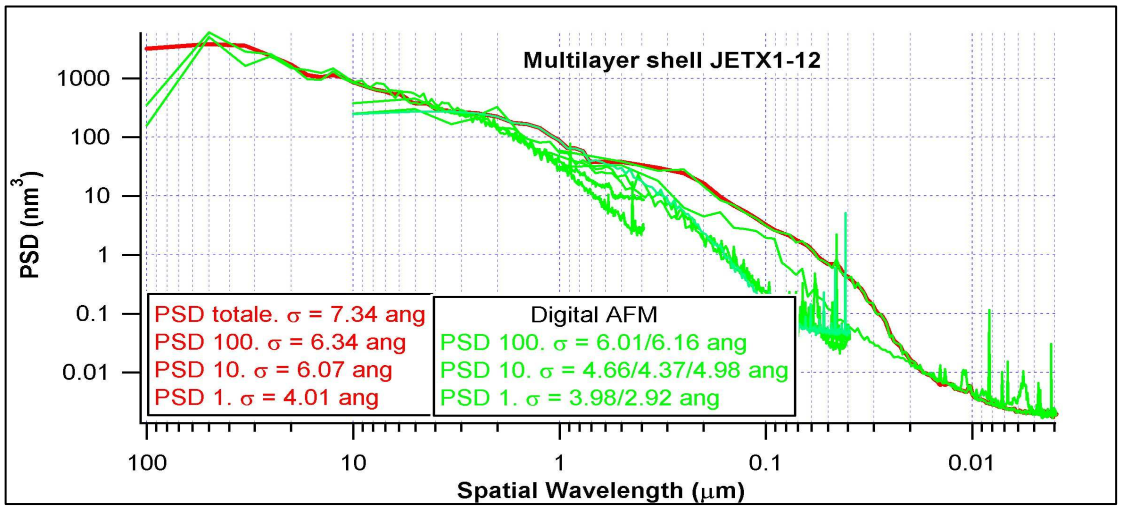

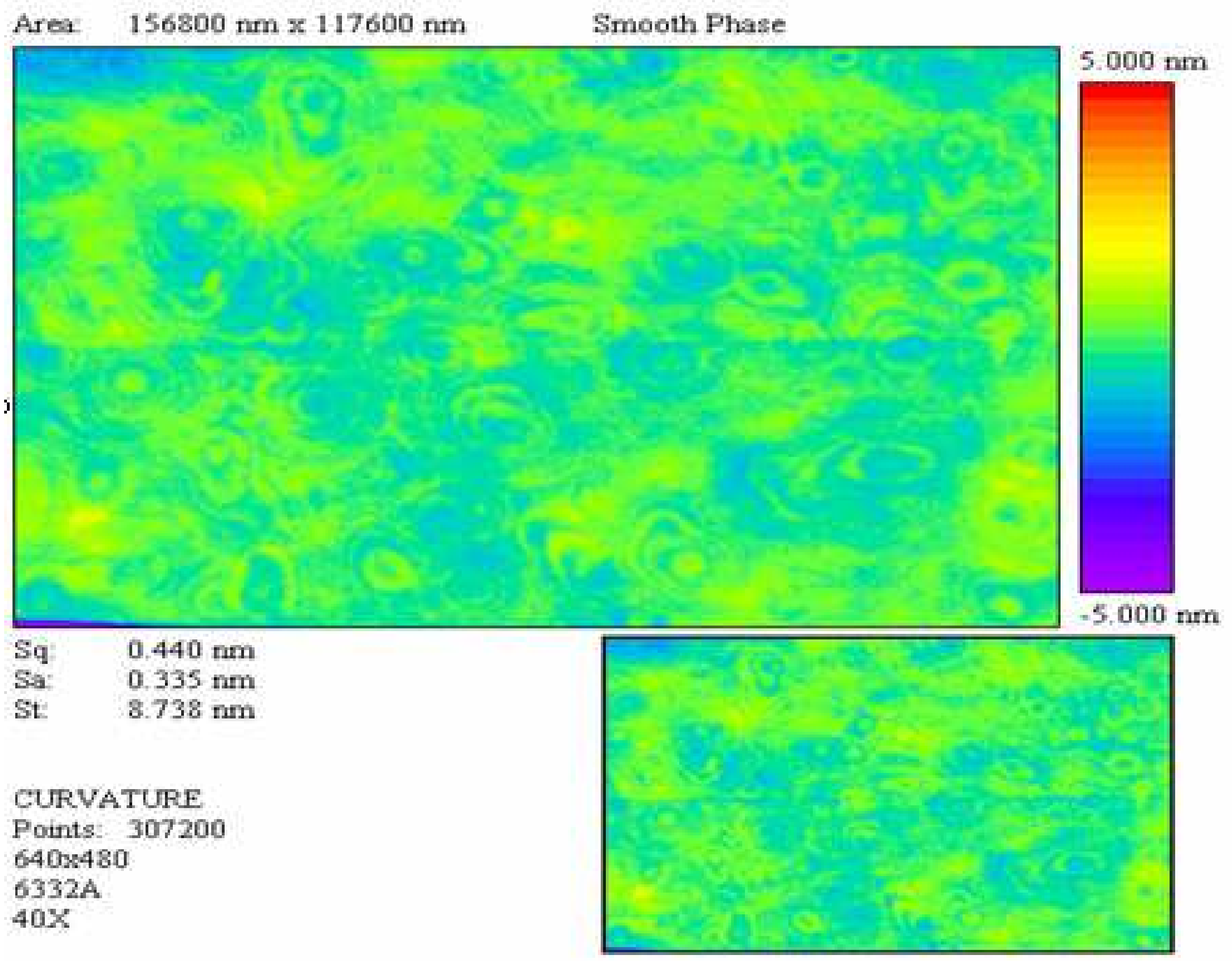

Mandrel surface mapping with PROMAP (credits: MediaLario techn.) after mirror shell replica: the same circular structures appear clearly.

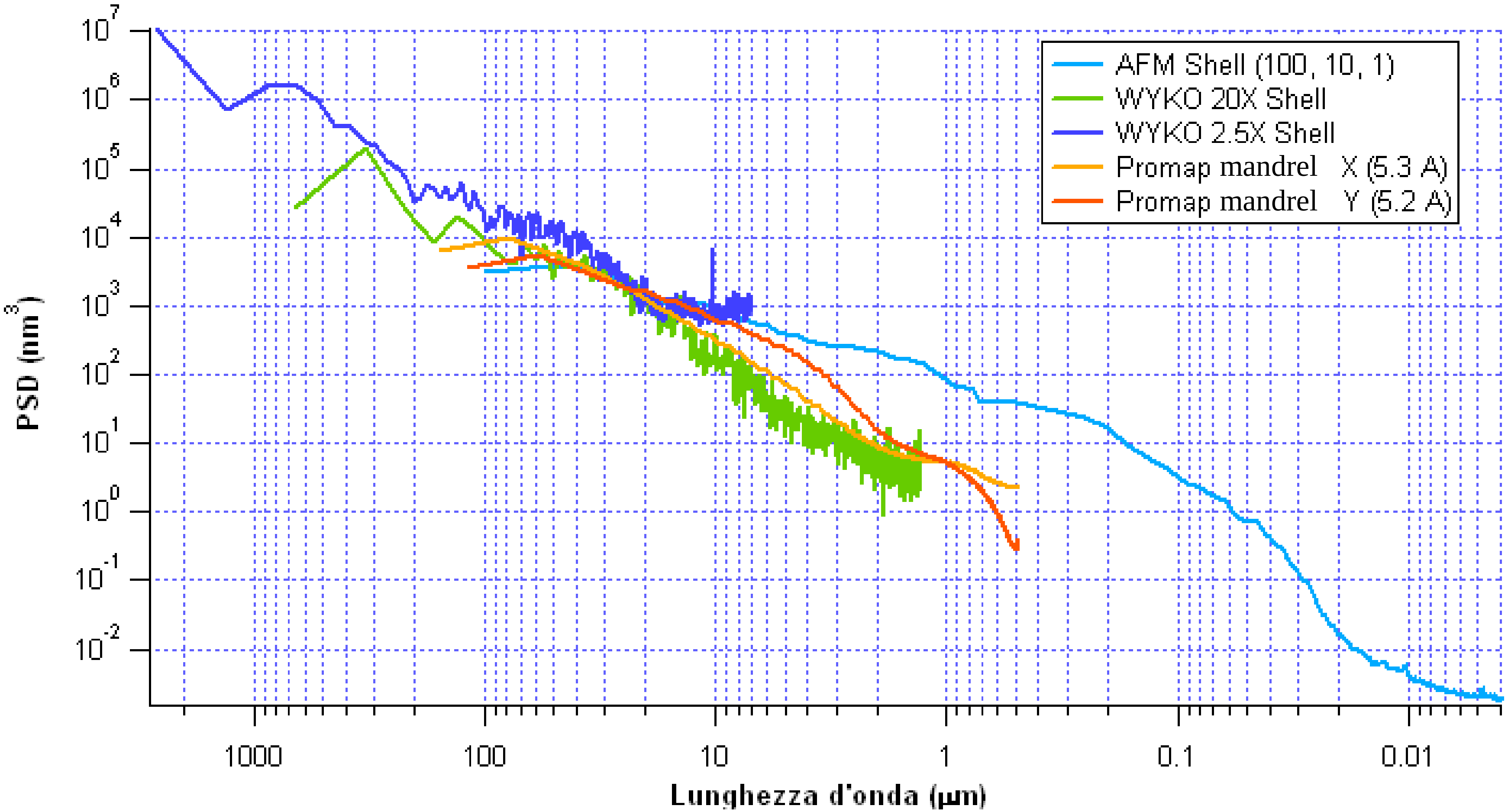

Mandrel surface mapping with PROMAP (credits: MediaLario techn.) after mirror shell replica: the PSD analysis shows a degradation of mirror shell in the spectral range 10 -1 µm with respect to the mandrel. At lower frequencies the mandrel features are replicated by the mirror shell surface.

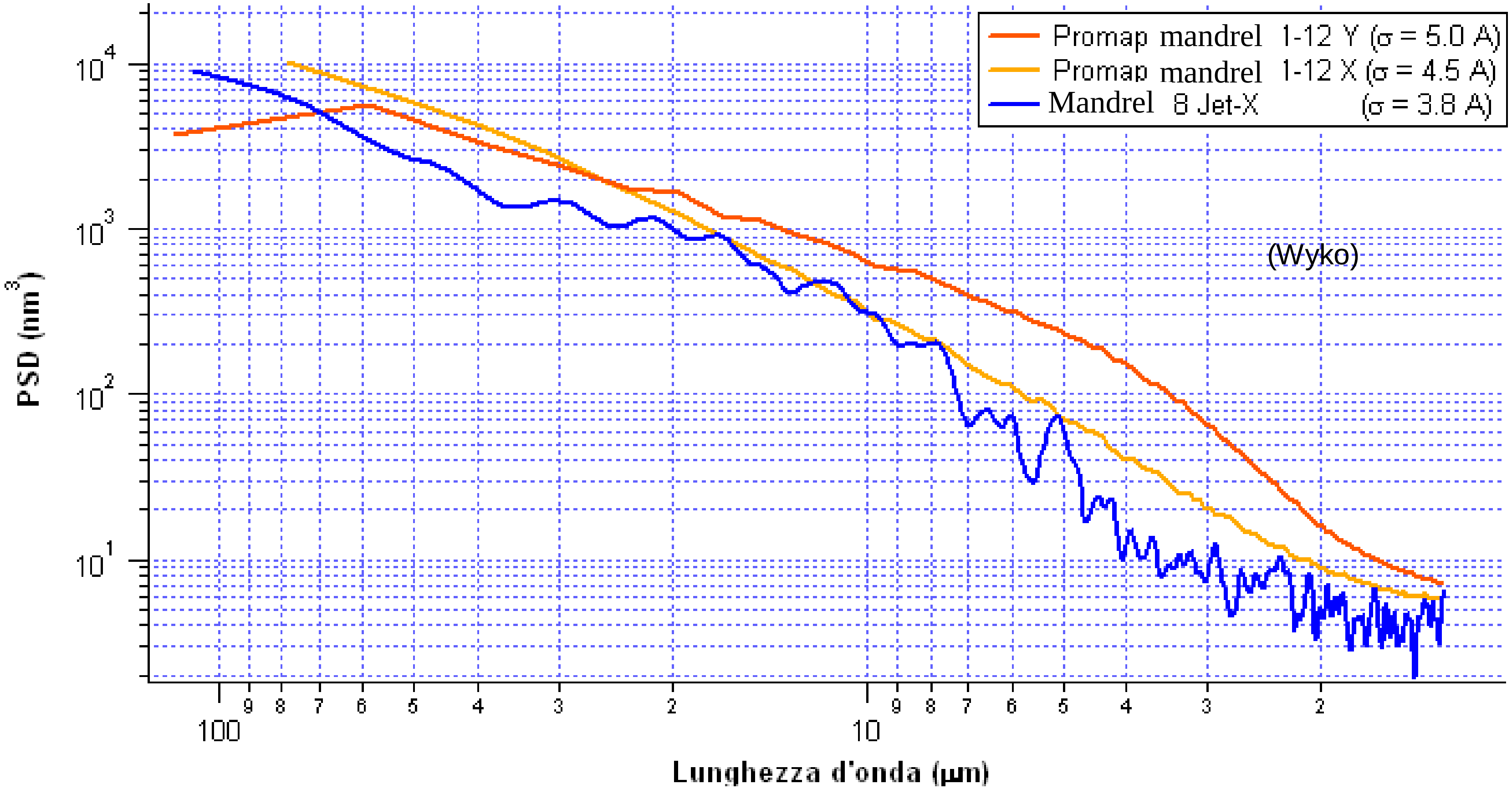

Mandrel surface mapping with PROMAP (credits: MediaLario techn.) after mirror shell replica: - the comparison with the Jet-X (WYKO) mandrel n. 8 shows also a general degradation of smoothness, likely caused by the iterated replicae.

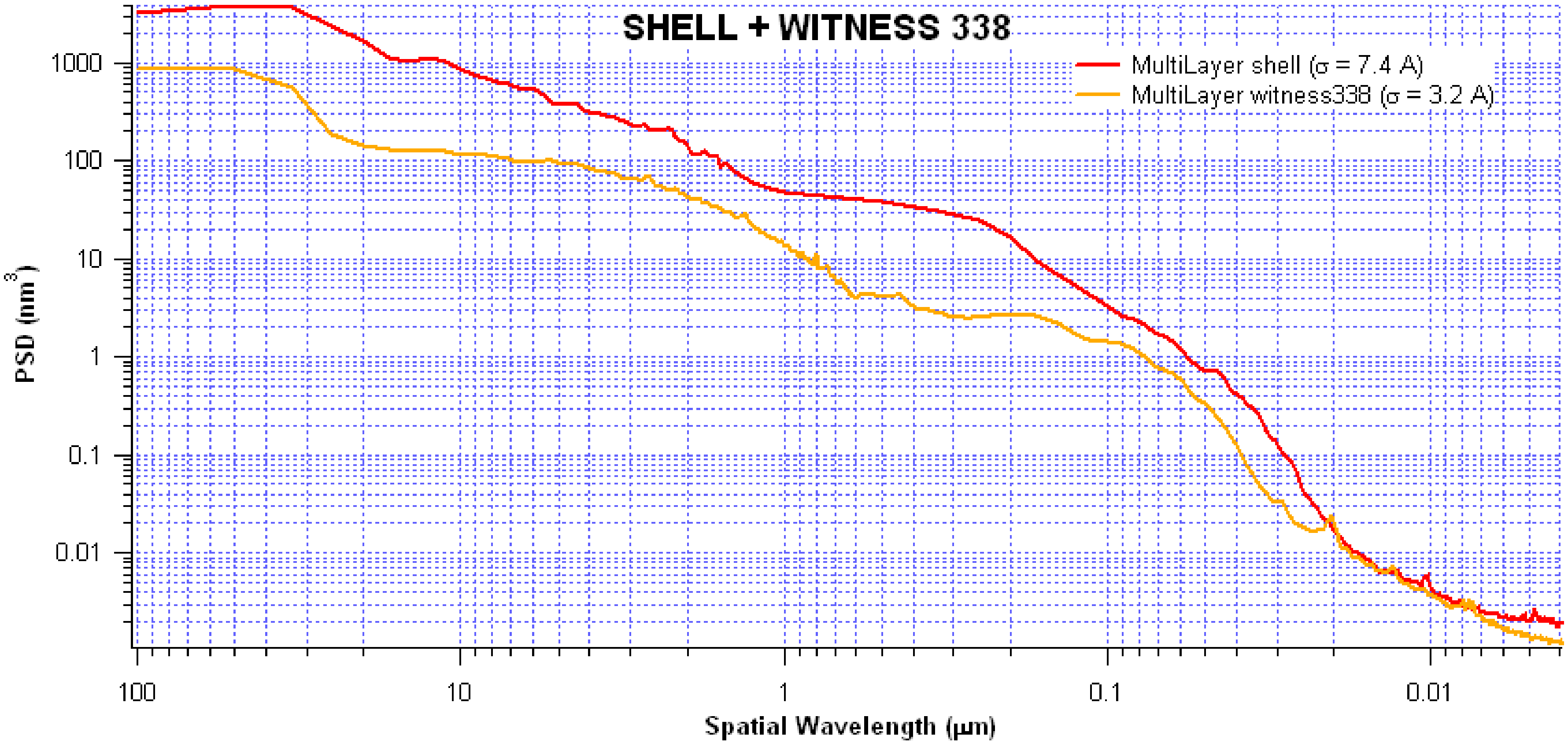

Comparison PSD Witness – Shell from AFM scans: the much better quality of substrate resulted in a better smoothness of multilayer surface.

Comparison coating surface – substrate for the mirror shell: the PSD of multilayer is slightly lower than the substrate (Ni + Au).

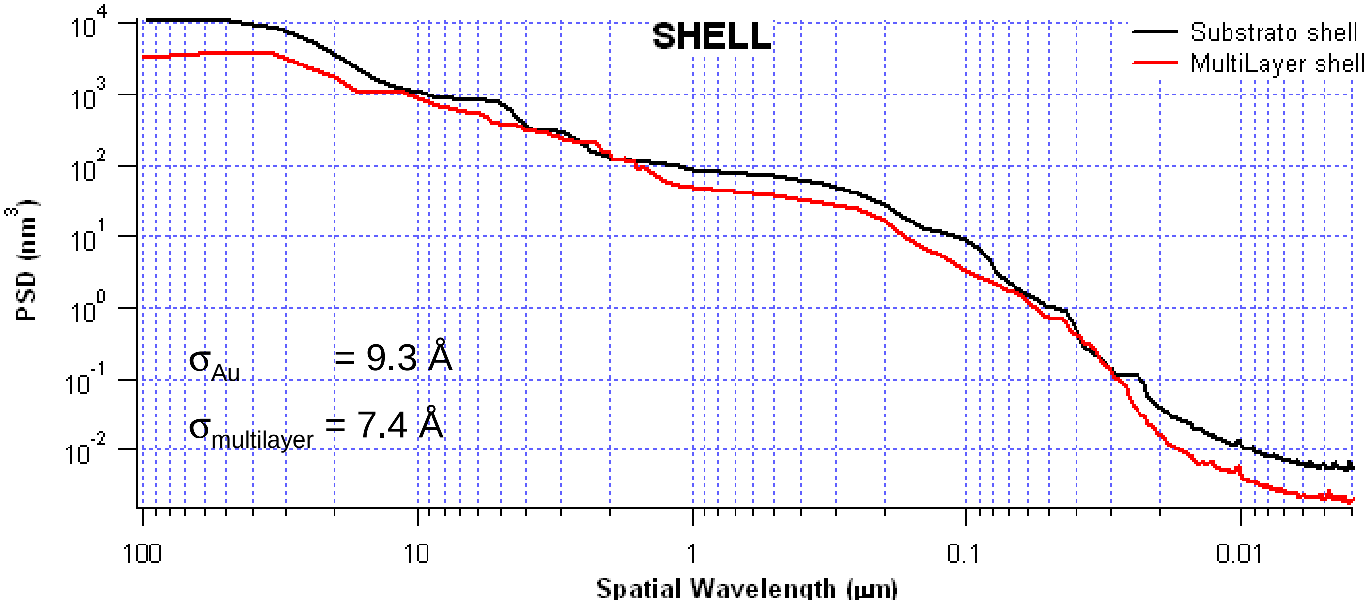

Comparison coating surface – substrate for the witness mirror: notice the growth of PSD in multilayer with respect to the substrate.

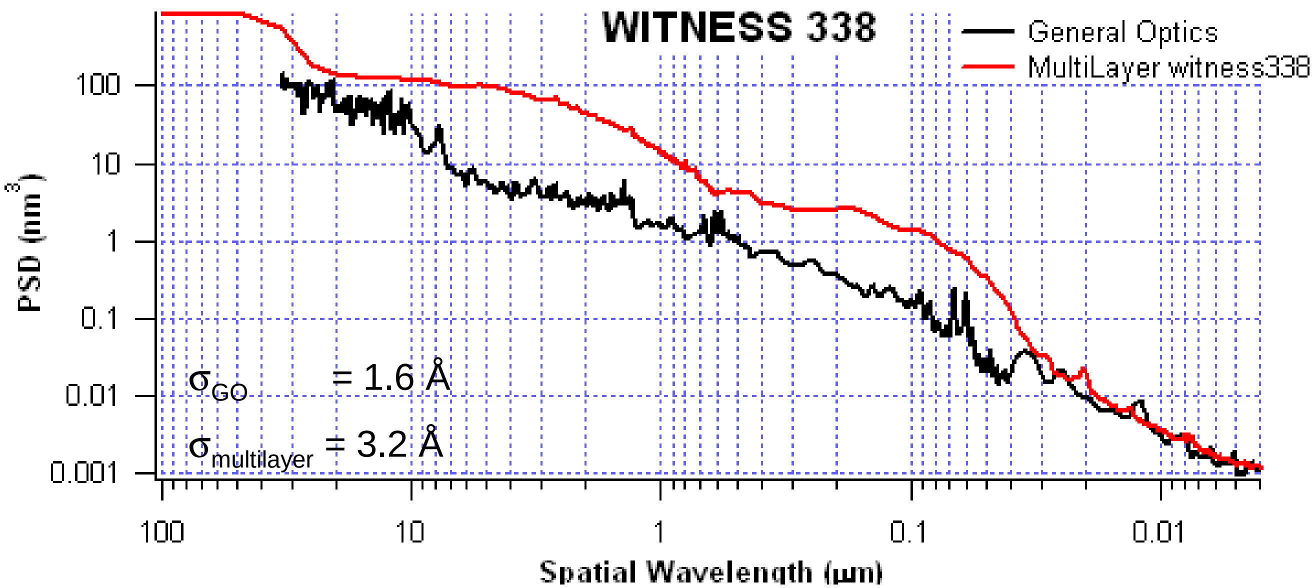

The difference of the two behaviours can be explained in terms of the same growth parameters (*Canestrari, Spiga, Pareschi 2005, SPIE 6266-41, in prep.*)

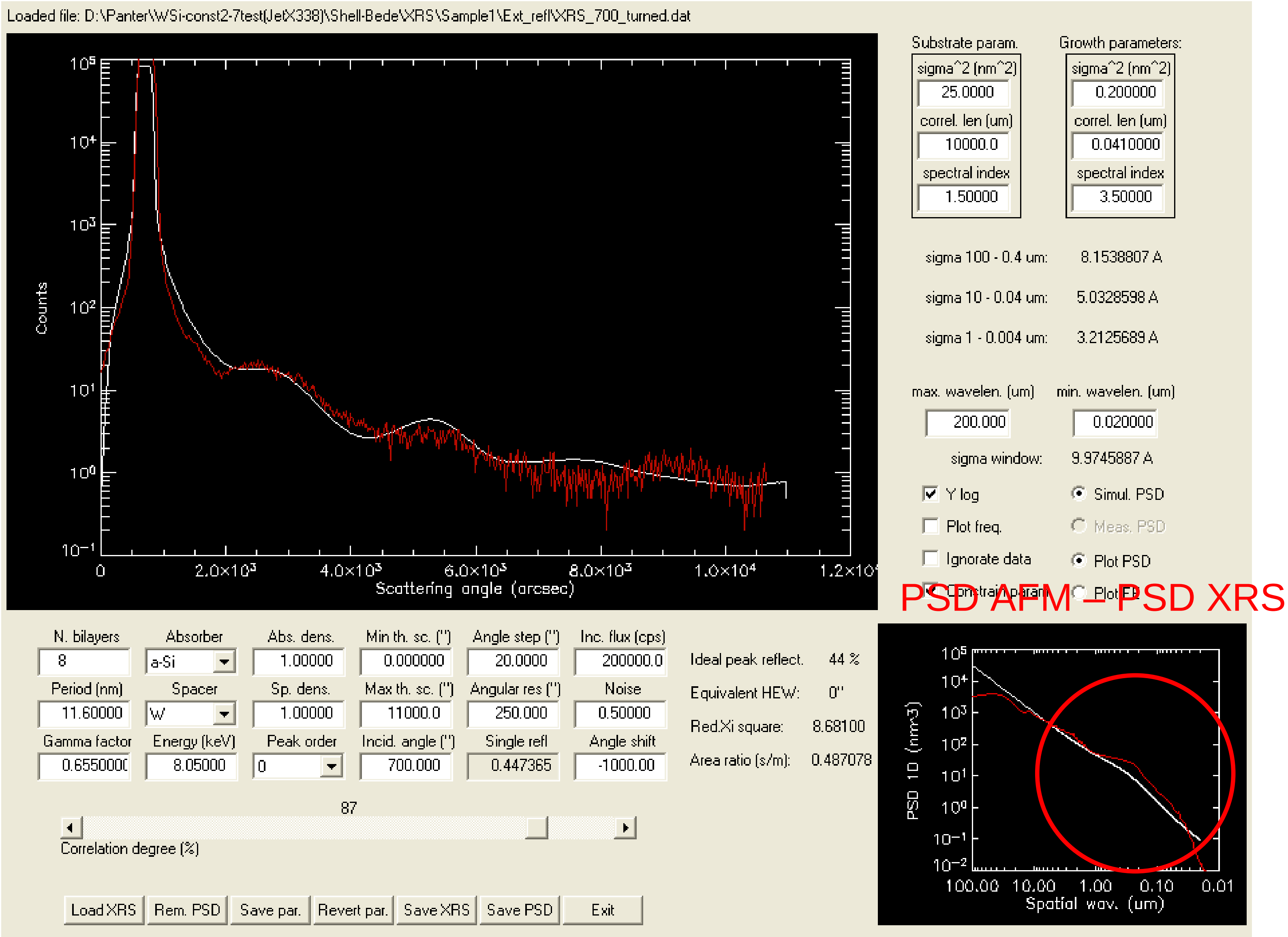

XRS measurement in external reflection regime (modelization with computer program *X.R.S.-M.An.* by *D. Spiga*). The scattering curve is in discrete agreement with AFM measured surface PSD.

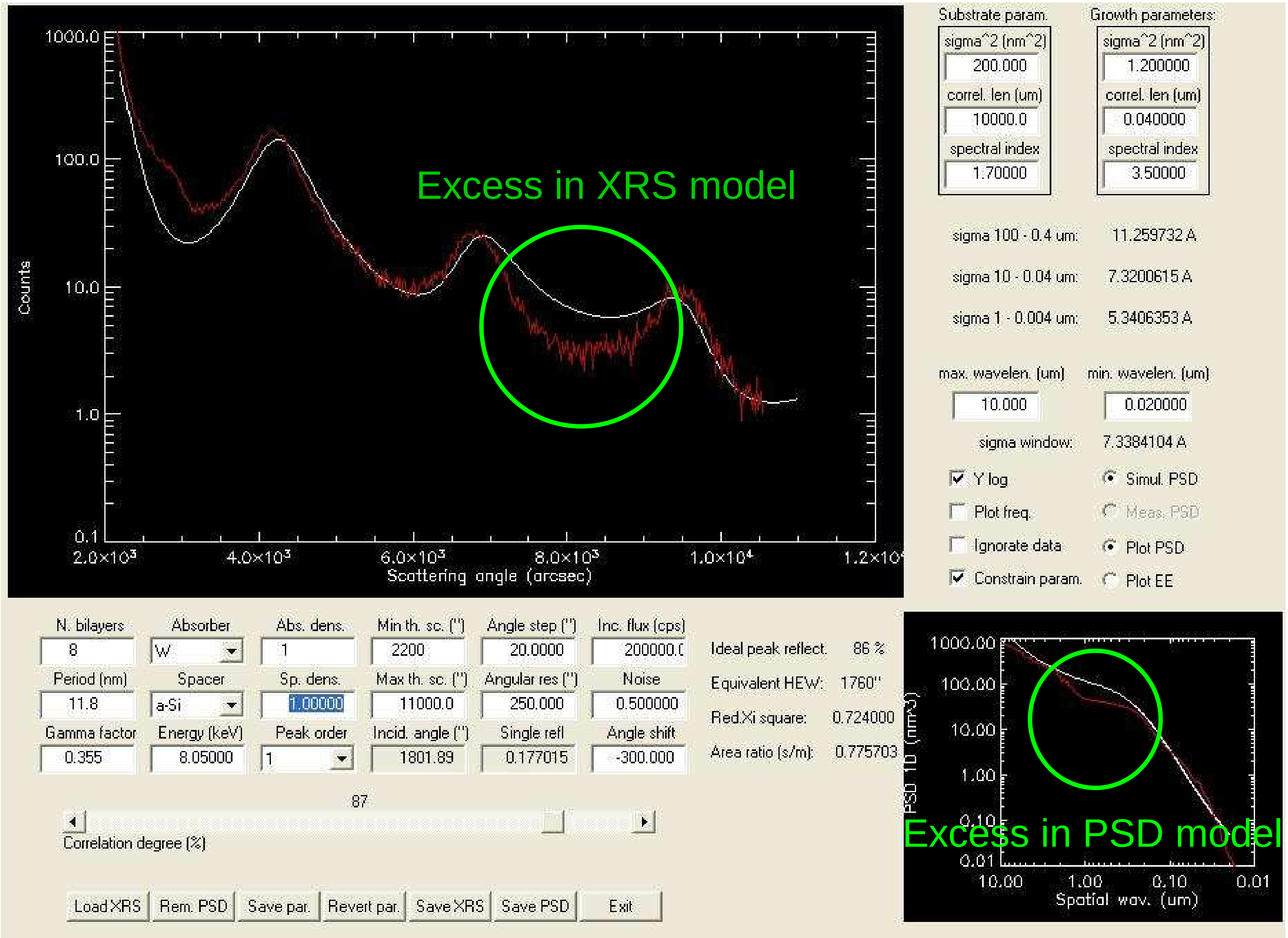

XRS measurement at the first Bragg peak: (modelization with computer program *X.R.S.-M.An.* by *D. Spiga*). The scattering curve is well modeled using a model PSD. The discrepancy is caused by the difficulty in an exact modeling of AFM PSD.

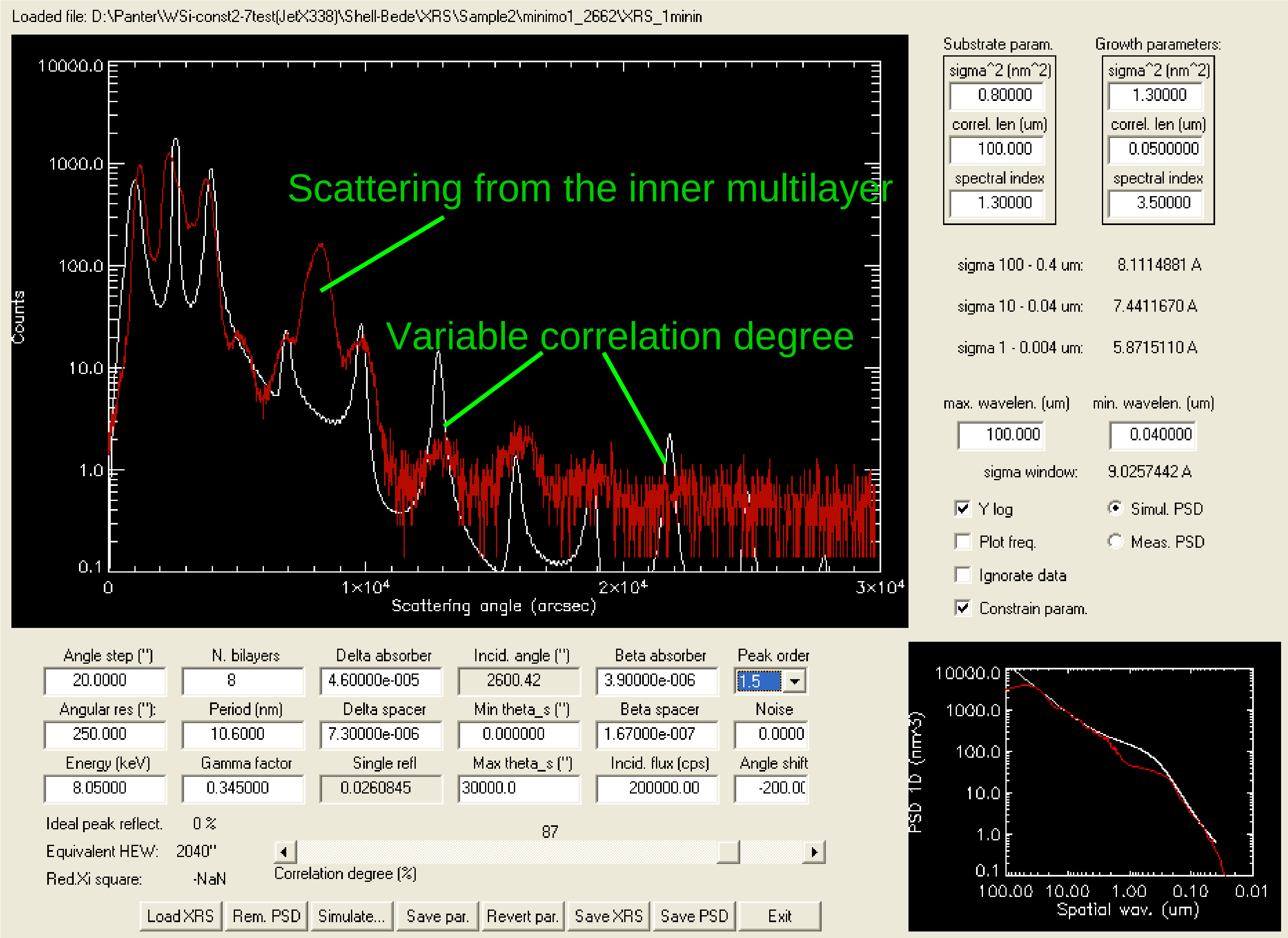

XRS measurement at the minimum after the first Bragg peak: (modelization with computer program *X.R.S.-M.An.* by *D. Spiga*). The scattering curve is well modeled using a model PSD. The implemented model does not include a variation of correlation degree with spatial frequency, which is probably present, nor the double multilayer stack, causing non-fitted XRS peaks.

Overview of roughness rms values measured with different methods

		100 µm	10 µm	1 µm
AFM witness:	σ =	2.8 Å	2.9 Å	2.0 Å
XRS witness (1 Br. p.):	σ =	-	3.15 Å	2.2 Å

Witness mirror: a good agreement is apparent between the AFM and XRS measurement.

		100 µm	10 µm	1 µm
AFM shell:	σ =	7.0 Å	5.8 Å	4.2 Å
XRS shell (rifl. ext.):	σ =	8.2 Å	5.0Å	3.2 Å
XRS shell (1 Br. p.):	σ =	11.3 Å	7.3 Å	5.3 Å
AFM substr. shell:	σ =	9.0 Å	7.1 Å	5.4 Å

Mirror shell: the agreement between the XRS in external reflection and AFM is apparent. The XRS measurement at the first Bragg peak is more similar to the substrate AFM, because it represents a proper average of the internal PSDs.

PSD shell overview (LTP+WYKO+AFM+ XRS)

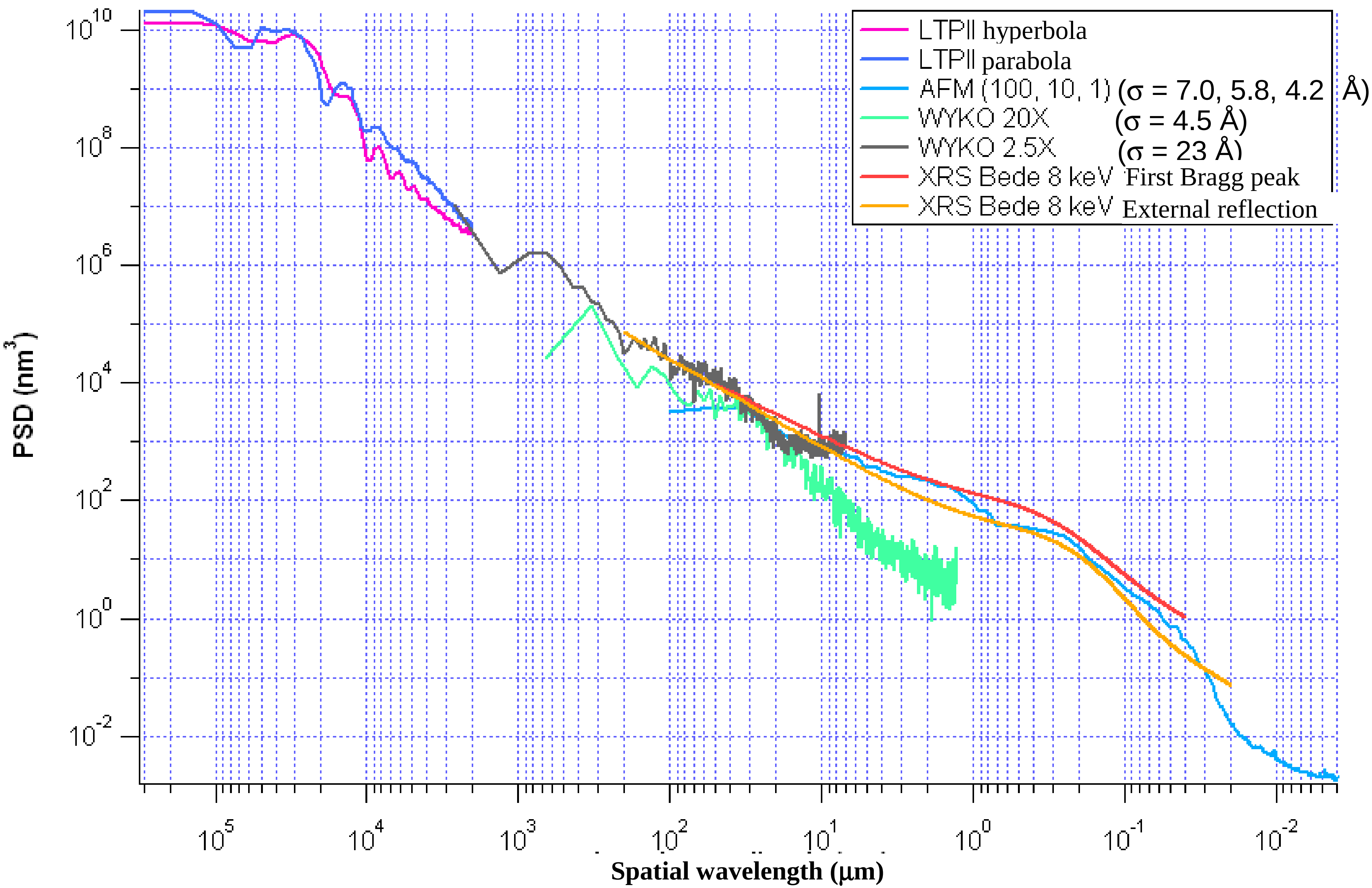

Notice: WYKO 20 x data can be not reliable below 10 µm

Comparison with Jet-X optic (1996)

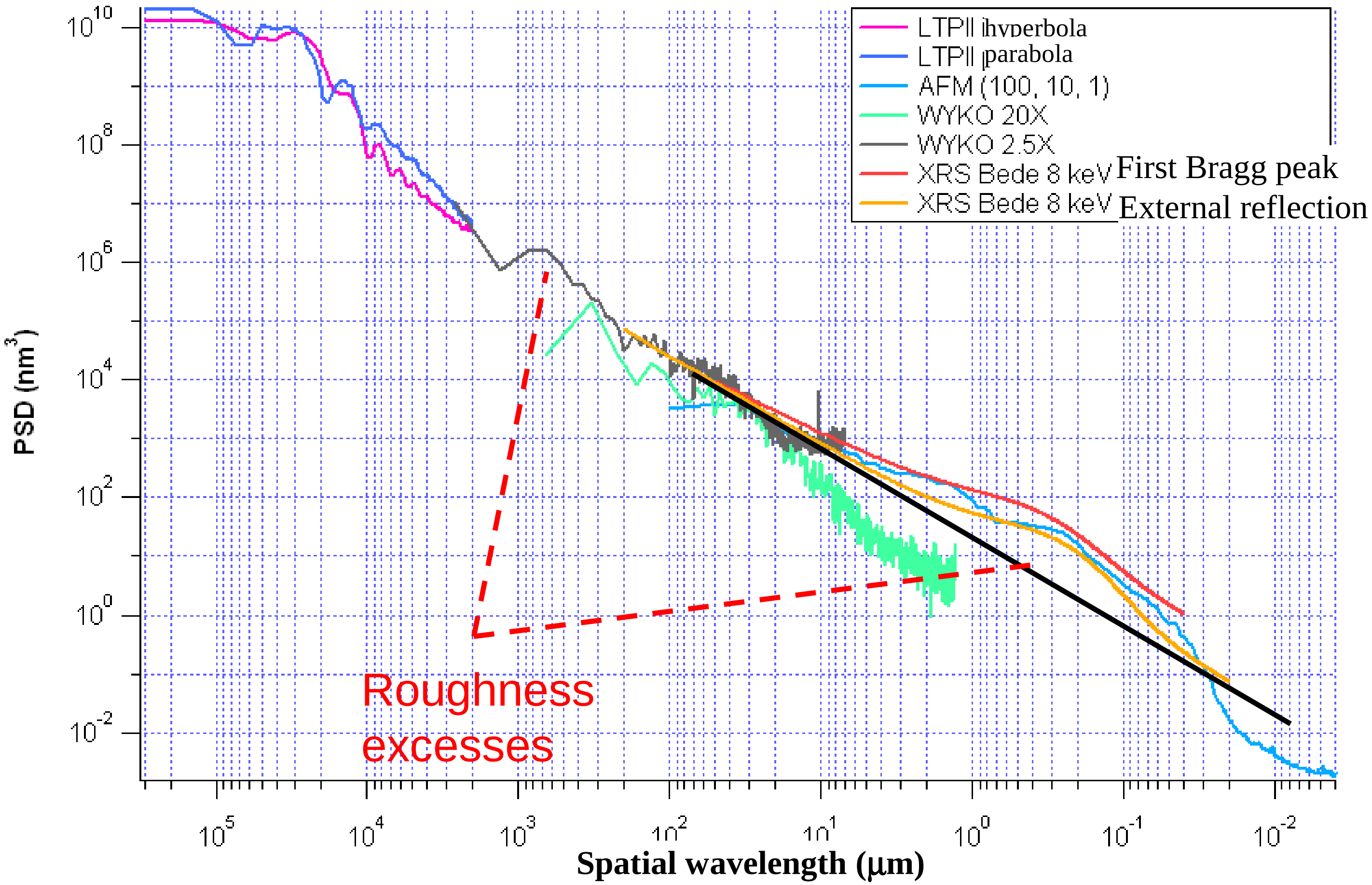

The black line here represents the PSD inferred from PANTER data of Jet-X optics calibration (Citterio et al., 1996). The inferred PSD is a power law with $n = 1.5$ and $\sigma(10\ \mu m) = 3.5$ Å.

PSD Comparison mirror shell /Au+Ni replica from GO

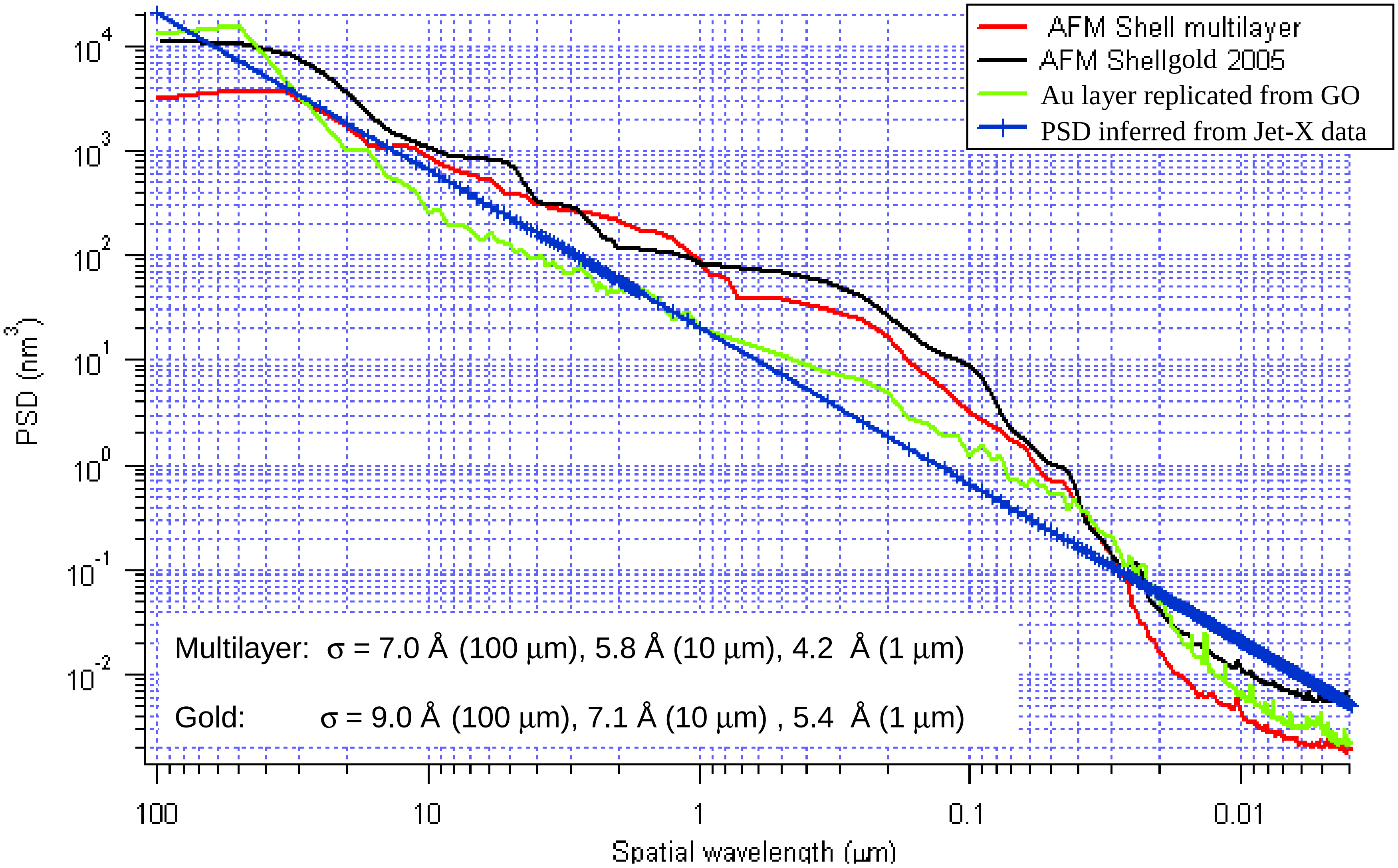

Measured HEW overview

• HEW figure errors (measured and simulated): 27”

Energy	Measured HEW (PSPC)	HEW excess due to X-ray scattering			Quadratic sum err. fig. + scatt.	Max Spatial period (XRS)
		totale	Core	Wings		
0.27 keV	45”	33”	22”	23”	43”	8 mm
1.49 keV	45”	22”	6”	21”	35”	2 mm
4.51 keV	55”	33”	6”	32”	43”	480 μm
8.05 keV	140”	87”	6”	86”	92”	100 μm

A 8.05 keV the HEW scattering is very important, but reflection does not occur in external reflection regime: the ordinary scattering theory is not applicable.

At 8.05 keV, at the PANTER actual angles the reflection falls at the first Bragg peak on the hyperbola and at the next minimum on the Parabola. At the minimum the reflectivity is low in specular direction but X-ray scattering is relevant anyhow in neighboring directions. This peak contrast effect could cause a HEW increase.

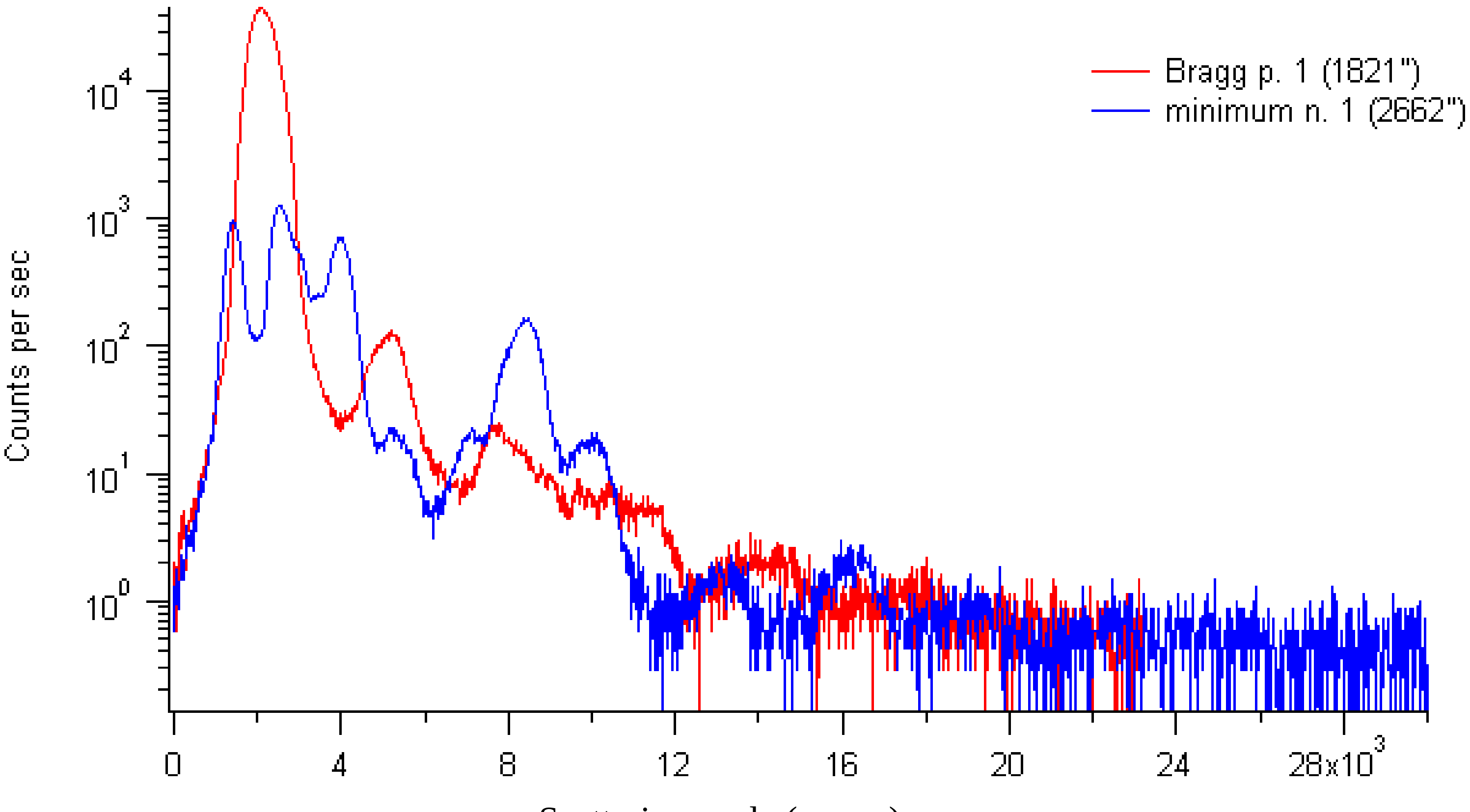

XRS measurement at 8.05 keV at the first peak and at the next minimum: the scattering intensity – referred to the peak value is much more relevant in the second case (at the reflection minimum).

7. TIS approach (Total Integrated Scattering)

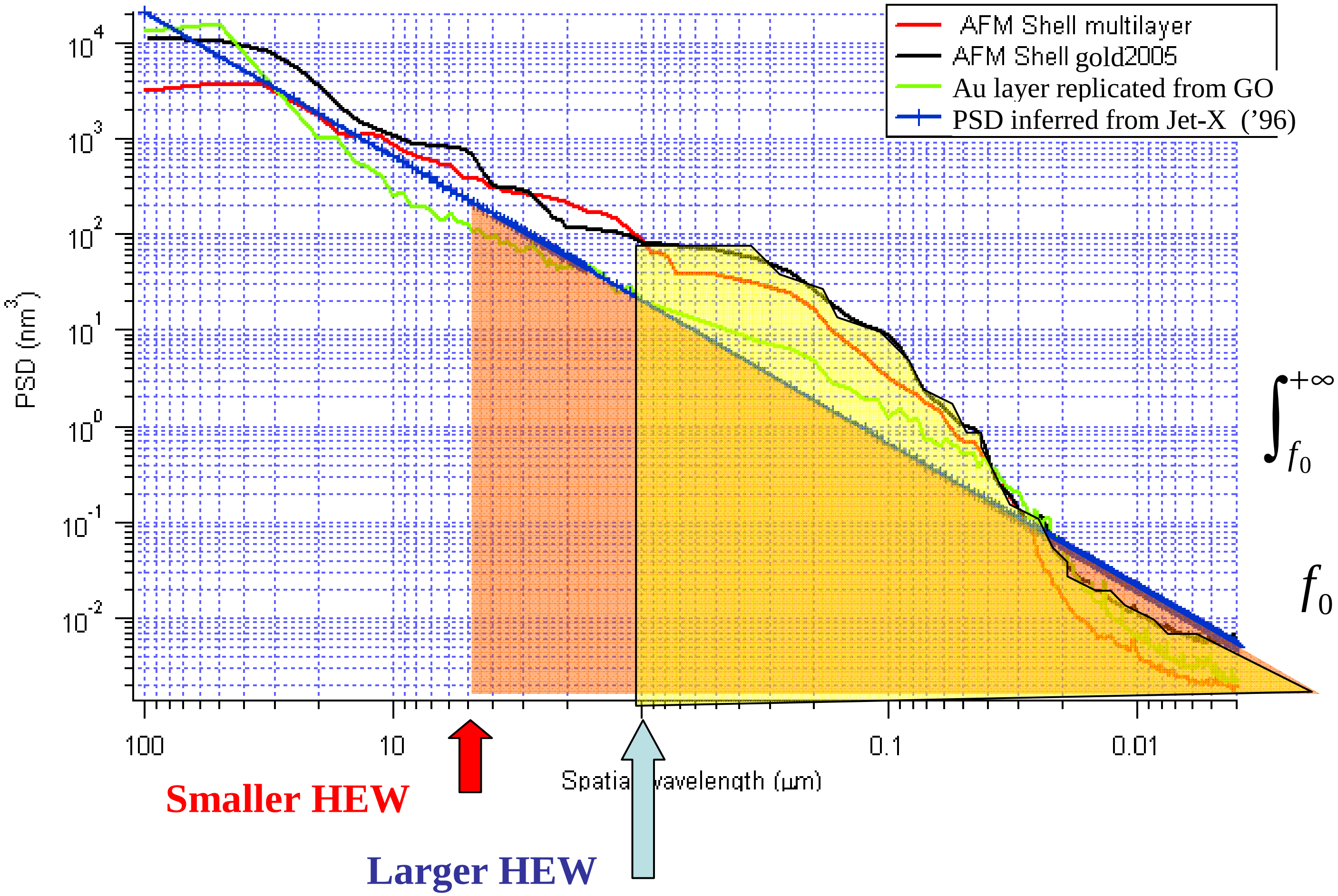

$$\int_{f_0}^{+\infty} I_{scatt}\, d\vartheta = \frac{I_{refl}}{2}$$

$$f_0 = \frac{HEW \sin\vartheta}{2\lambda}$$

This approach assumes that we integrate the PSF curve from outside to the center up to reaching the condition of a Total Integrated Scattering equal to the half of the reflected intensity. The corresponding stop frequency is simply related to the HEW. Bumps in the PSD cause an increase of HEW.

TIS approach results:

The measured PSD is too low to reach the large measured HEW values (in scattering component) at low energies (0.27, 1.49, 4.51 keV), while at 8.05 keV returns an HEW compatible with the observed one. At very low energies (0.27 keV) the PSD is not extended enough to reach the half of reflected power (analysis by R. Canestrari).

Energy	Measured HEW excess, shell 338 scattering only **from deconvolution**	TIS results from Shell PSD	
		HEW	Max spatial wavelength
0.27 keV	33”	-	-
1.49 keV	22”	5.7”	9 mm
4.51 keV	33”	17.5”	660 μm
8.05 keV	86”	95”	64 μm

These HEW seem to be mainly related to the low- frequency roughness: these values were obtained assuming n = 1.7, A = 220 nm^2

TIS approach results:

HEW inferred from Jet-X PSD (derived from Citterio et al.)

Energy	Measured HEW excess shell 338, Scattering only **from deconvolution**	TIS results from Jet-X PSD	
		HEW	Max spatial wavelength
0.27 keV	33”	-	-
1.49 keV	22”	-	-
4.51 keV	33”	5.7”	2.5 mm
8.05 keV	86”	22”	300 μm

The PSD of original Jet-X returns much less HEW than the actual measured PSD for shell 338.

TIS approach results (comparison):

Measured HEW and calculated from original Jet-X PSD, from the shell 338 PSD and from Au+ electroformed Ni sample (replicated from GO). HEW decrease for improved surface smoothness. At low energies the HEW could not be determined for the smoothest surfaces.

Energy	Scattering HEW term (deconvolved)	HEW from TIS analysis		
		Measured PSD AFM+ WYKO 2.5 + LTP II	**Jet-X power law**	**Au + Ni replicated from GO**
0.27 keV	33"	-	-	-
1.49 keV	22"	5.7"	-	-
4.51 keV	33"	17.5"	5.7"	3.3"
8.05 keV	86"	95"	22"	17.5"

8. Hyperbola - parabola convolution approach

In order to simulate the real scattering from the optic in total external regime, using an IDl routine written by D. Spiga. It implements the convolution of scattering diagram of parabola with that of hyperbola, starting from a definite PSD scheme of mirror surface.

Even in this case the low frequency contribution (1 mm – 100 mm) is important.

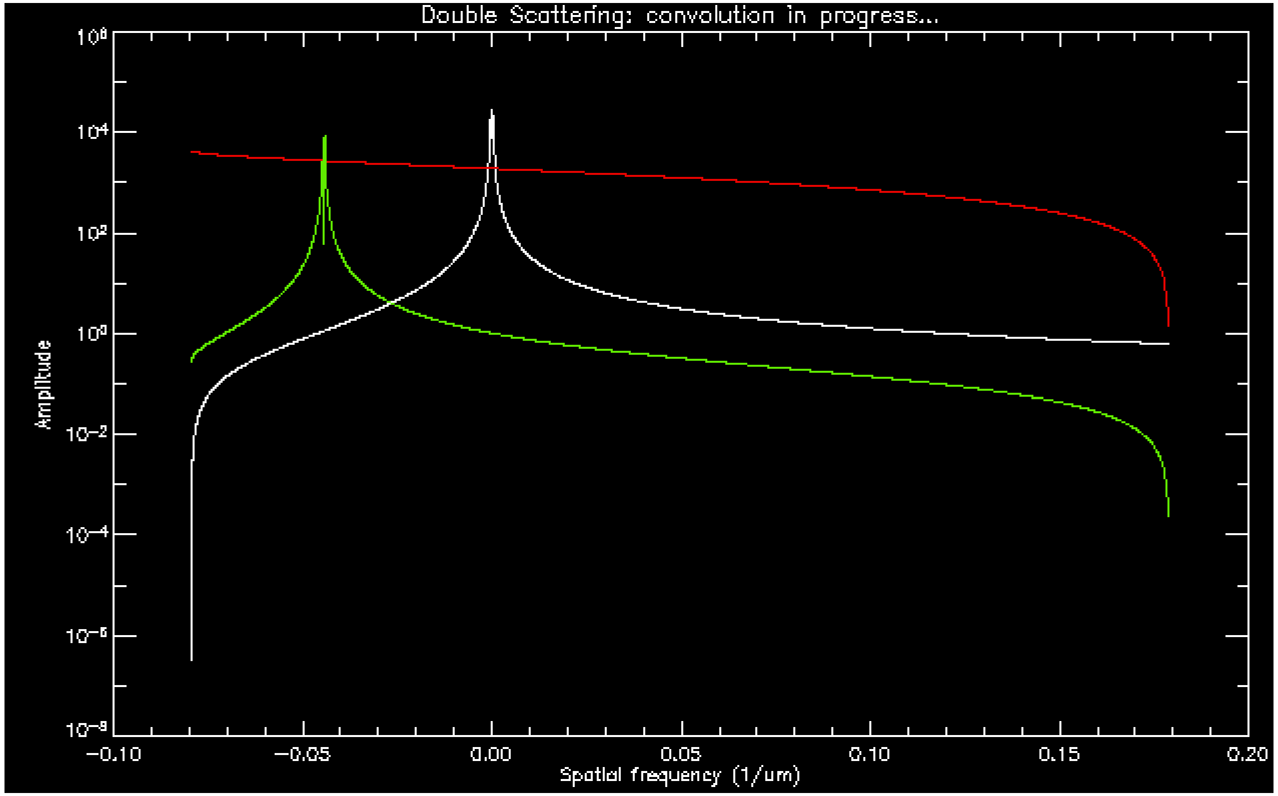

Convolutive approach results: total HEW

Assumed a figure error HEW of 27”

Energy	HEW measured at PANTER	Convolution results			
		Measured PSD AFM+ WYKO 2.5 + LTP II 100, 10, 1 μm 7.0, 5.8, 4.2 Å	PSD measured + low-frequency extrapolation*	Jet-X power law	Au + Ni replicated from GO
0.27 keV	45”	29”	30”	29”	28”
1.49 keV	45”	32”	44”	30”	30”
4.51 keV	55”	56”	67”	35”	32”
8.05 keV	137”	70”	69”	39”	34”

* The PSD has been extrapolated to low frequencies in order to derive the HEW at low energies: the achieved agreement requires indeed, a steeper PSD than the probable one (with a spectral index of 1.5).

Convolutive approach results: scattering contribution to HEW

Energy	HEW measured at PANTER	Convolution results			
		Measured PSD AFM+ WYKO 2.5 + LTP II 100, 10, 1 μm 7.0, 5.8, 4.2 Å	**PSD measured + low-frequency extrapolation***	**Jet-X power law**	**Au + Ni replicated from GO**
0.27 keV	33”	8”	8”	8”	5”
1.49 keV	22”	11”	21”	9”	8”
4.51 keV	33”	35”	47”	12”	10”
8.05 keV	87”	47”	49”	15”	11”

* The PSD has been extrapolated to low frequencies in order to derive the HEW at low energies: the achieved agreement requires indeed, a steeper PSD than the probable one (with a spectral index of 1.5).

Conclusions

1) We could not explain the unexpectedly large value of HEW measured at 0.27 keV
2) At higher energies the scattering contribution *seems* to be more or less "justified" by roughness measurements on the basis of the convolutive approach.
3) The method can be apparently be used – after further verifications – for future simulations of optics performances
4) Multilayer scattering has been interpreted on the basis of a simple model and will be implemented in the convolution program to extend the method to high energies.
5) If we except some discrepancies, the mandrel smoothness has been degradated by iterated replicae
6) A mandrel roughness reduction should bring us to a scattering mitigation that would lead the HEW to values nearer to those measured with the UV optical bench.